UvA-DARE (Digital Academic Repository)

MaQuIs—Concept for a Mars Quantum Gravity Mission

Wörner, L.; Root, B.C.; Bouyer, P.; Braxmaier, C.; Dirkx, D.; Encarnação, J.; Hauber, E.; Hussmann, H.; Karatekin, Ö.; Koch, A.; Kumanchik, L.; Migliaccio, F.; Reguzzoni, M.; Ritter, B.; Schilling, M.; Schubert, C.; Thieulot, C.; Klitzing, W.V.; Witasse, O.

Citation for published version (APA):

Wörner, L., Root, B. C., Bouyer, P., Braxmaier, C., Dirkx, D., Encarnação, J., Hauber, E., Hussmann, H., Karatekin, Ö., Koch, A., Kumanchik, L., Migliaccio, F., Reguzzoni, M., Ritter, B., Schilling, M., Schubert, C., Thieulot, C., Klitzing, W. V., & Witasse, O. (2023). MaQuIs—Concept for a Mars Quantum Gravity Mission. *Planetary and Space Science*, *239*, Article 105800. https://doi.org/10.1016/j.pss.2023.105800

MaQuIs—Concept for a Mars Quantum Gravity Mission

L. Wörner [g,*,1], B.C. Root [b,1], P. Bouyer [c,1], C. Braxmaier [a,d,1], D. Dirkx [b,1], J. Encarnação [b,1], E. Hauber [e,1], H. Hussmann [e,1], Ö. Karatekin [f,1], A. Koch [g,1], L. Kumanchik [a,1], F. Migliaccio [h,1], M. Reguzzoni [h,1], B. Ritter [f,1], M. Schilling [g,1], C. Schubert [g,1], C. Thieulot [i,1], W.v. Klitzing [j,1], O. Witasse [k,1]

[a] *German Aerospace Center, Institute for Quantumtechnologies, 89081 Ulm, Germany*
[b] *Delft University of Technology, Department of Space Engineering, Delft, The Netherlands*
[c] *University of Amsterdam, Eindhoven University of Technology, The Netherlands*
[d] *Universität Ulm University, Institute of Microelectronics, Albert-Einstein-Allee 43, 89081 Ulm, Germany*
[e] *German Aerospace Center, Institute of Planetary Research, 12489 Berlin, Germany*
[f] *Royal Observatory of Belgium, Brussels, Belgium*
[g] *German Aerospace Center, Institute for Satellite Geodesy and Inertial Sensing, Callinstrasse 30b, 30167 Hannover, Germany*
[h] *Politecnico di Milano, Department of Civil and Environmental Engineering, Milan, Italy*
[i] *Mantle dynamics group, Utrecht University, The Netherlands*
[j] *Institute for Electronic Structure and Laser, Foundation for Research and Technology Hellas, Heraklion, Greece*
[k] *European Space Agency, ESTEC, Noordwijk, The Netherlands*

ARTICLE INFO

ABSTRACT

The aim of this paper is to present the concept of a dedicated gravity field mission for the planet Mars, the Mars Quantum Gravity Mission (MaQuIs).

The mission is targeted at improving the data on the gravitational field of Mars, enabling studies on planetary dynamics, seasonal changes, and subsurface water reservoirs.

MaQuIs follows well known mission scenarios, currently deployed for Earth, and includes state-of-the-art quantum technologies to enhance the gained scientific signal.

Plain text summary

MaQuIs is a mission and technology concept to map the gravity field of Mars to investigate subsurface structures and observe temporal changes. Consequently, MaQuIs yields information on the development of the planet and allows a deeper view into the structure and internal processes than ever before. For this purpose, MaQuIs deploys quantum mechanical systems to measure the gravity field following successful missions such as GRAIL and GRACE on the Moon and Earth respectively.

1. Introduction

The study of planets is interesting for several different reasons, such as planetary composition, evolution, and density, surface properties, prospecting, and comparative planetology (Glassmeier, 2020). One major subject of study is the search for water in planets outside Earth (Nazari-Sharabian et al., 2020; O'Rourke et al., 2020; Peddinti and McNamara, 2019; Bibring et al., 2006). Especially important in this case is the abundance of liquid water and subsurface ice, since it could foster life and support a potential landing party.

In addition to static water distribution on a planet, shifts and dynamics in the planets density, are of high importance. The comparison to Earth's dynamics, allows to deepen the understanding of both the Earth's and the planets dynamics and consequently study phenomena such as climate change, seismic activity, seasonal variations, or volcanic eruptions. With those data available, inner structures can be modelled and predictions made (Banerdt et al., 2020).

For this purpose different missions, orbiting planets, landing on planets and comets, and samples return missions, have been carried out in the past (Breuer et al., 2022).

Here, we discuss the concept and technology necessary for a Mars Quantum Gravity Mission, MaQuIs, which aims at improving the current knowledge of the gravitational field map of Mars and thereby enabling research of seasonal changes, planetary dynamics, and subsurface water occurrences.

---

* Corresponding author.
  E-mail address: lisa.woerner@dlr.de (L. Wörner).
[1] All authors contributed equally to the manuscript.

Similar to Earth and Lunar satellite gravimetry missions, such as GRAIL (Zuber et al., 2013) and GRACE (Tapley et al., 2004), static occurrences, marked by differences in density as well as dynamical processes are detectable from orbit. Such a dedicated gravity mission would improve the static gravitational field model of Mars, determine its temporal components, and allow to pinpoint the distribution of water with a higher accuracy then current orbital missions. Additionally, a more detailed knowledge of the gravitational field distribution paves the way to improving not only the depth resolution of subsurface lakes and their distribution around the entire planet, but also to identify and characterize other buried mass structures like hidden impact craters (Frey et al., 2002) and magma chambers (Mari et al., 2020; Broquet and Andrews-Hanna, 2022).

Recently, missions have been proposed for low Mars orbit to improve existing geodetic and remote sensing data-sets using current techniques of gravity field determination and orbit determination based on Doppler tracking and inter-satellite radio links (Genova, 2020; Oberst et al., 2022).

Landers can support such global missions, as their resolution for a specific area is increased on the expense of being restricted to a limited area.

A dedicated global gravity mission would allow to identify interesting sites for further robotic ground based investigation, including possible drilling sites and to prepare human exploration with identification of potential landing sites with local sources for In-Situ Resource Utilisation (ISRU).

MaQuIs will follow the mission design of GRACE (Tapley et al., 2004), GRICE (Lévèque et al., 2021), CARIOQA (Lévèque et al., 2022), and GRAIL (Zuber et al., 2013). MaQuIs will deploy quantum mechanical systems to enable the gravity field measurement. This increases the resolution of the gravitational field map, as discussed for similar missions for Earth (Carraz et al., 2014; Lévèque et al., 2021, 2022). Additional optomechanical sensors and optical link technologies enable the proposed mission. In the following, the mission is outlined, giving an overview over scientific goals, system level requirements, an envisioned mission design, and orbital considerations.

2. Scientific goals

Gravitational data can be used to study the surface and subsurface of the planet leading to improved understanding of the Martian crust and lithosphere (Beuthe et al., 2012). Such data also holds the potential to investigate dynamic surface processes, such as atmospheric seasonal changes, appearance of ice sheets, and large scale erosion of the Martian surface.

While dynamic surface effects can be observed by optical means, such as spectroscopy and imagery, subsurface effects and density distributions require additional instruments. With seismographs and radiography being two deployed possibilities, the study of the gravitational field supported by information on the visible shape of the planet enables the study of static and dynamic processes under the planet's surface. The accuracy of both information, the imagery and the gravitational field data, determine the accuracy of predictions and the quality of models of the internal structure and planetary composition. Additionally, sufficiently accurate measurements allow the identification of areas of high or low mass density and their dynamics, leading to the identification of interesting regions and determination of future landing sites.

2.1. Gravity maps of Mars

Over the past decade, Mars has taken more and more of the spotlight. Several missions to investigate local and global properties of the Red Planet have been successfully operated, one of the latest being Perseverance (Jacobstein, 2021). Future planned missions to Mars

and its moons include orbiters and landers (Muirhead et al., 2020). Consequently, Mars is already orbited by several different satellites.

From orbits determined by Doppler tracking observations, the current resolution of the gravitational field map of Mars is in the order of 115 km at ground level (Konopliv et al., 2011, 2016; Genova et al., 2016). Fig. 1 shows the gravity anomalies on the areoid, the planetary geoid of Mars, up to degree and order 120. A large correlation of the field is seen with the small scale topography. The dichotomy observed in the topography of Mars is missing in the gravity anomalies, suggesting some form of local isostasy in the sub-surface. Another global gravity feature stands out, related to the volcanic region, the Tharsis Rise. A large positive gravity anomaly (approximate 300 mGal) situated at the Tharsis Rise is surrounded by a ring of negative gravity anomaly (approximate −300 mGal), seemingly detached from any geologic feature. A feature that also stands out in the degree and order (d/o) 2–3 of the spherical harmonic coefficients that capture the spectral content of the gravitational field.

Fig. 2 shows the degree variances (or spectral signatures) of several Martian gravity field models with its uncertainty estimates. We compare here the four most used versions of the Martian gravitational field: GGMRO-95 (Konopliv et al., 2006), GMM-3-120 (Genova et al., 2016), JGMRO-120d (Konopliv et al., 2016), and JGMRO-120F models (Konopliv et al., 2020). All four fields coincide up to degree and order 60, where the oldest model GGMRO-95 starts to divert. The newer models include more and lower orbital data improving the resolution and accuracy of the model. The dashed lines denote the error estimates of these models. Around degree 100 the error estimates cross the actual model content, which shows that the models can only be trusted up to degree 100, which stands for a spatial resolution of 115 km.

The observed orbits used to construct these gravitational models need to be corrected for non-conservative accelerations acting on the satellite, like atmospheric drag and solar radiation pressure, prior to or during gravity field recovery (Konopliv et al., 2006). Incorrect modelling of these effects will leak into the gravity field models as clearly shown by the improved consistency in results obtained by Genova et al. (2016) after incorporating a more detailed atmosphere model. A dedicated gravity field mission will not only result in an improved gravity field model of Mars, but also give insights in better atmospheric models of Mars (Doornbos, 2012), which is in turn important for interpreting temporal gravity signatures (Petricca et al., 2022).

2.2. Water on Mars

2.2.1. Liquid water on Mars

Abundant morphological and mineralogical evidence points to large amounts of liquid water that must have been present at the surface of early Mars (Carr and Head, 2015; Bibring et al., 2006). Large parts of that early reservoir have been lost to space (Jakosky, 2021), and today, the largest known part of the remaining martian water is present in the polar caps (Byrne, 2009), in near-surface ice deposits in high and mid-latitudes (Holt et al., 2008; Dundas et al., 2021), and as water in hydrated minerals (Carter et al., 2023). However, it cannot be excluded that liquid water is present even today in the subsurface in the form of deep groundwater (Grimm et al., 2017) underlying a thickening cryosphere (Clifford et al., 2010). In fact, radar measurements suggest that a briny layer of liquid water may exist beneath a 1.5 km-thick part of the south polar ice cap (Lauro et al., 2021), however, this interpretation of the data is debated (Smith et al., 2021; Bierson et al., 2021). If there are any aquifers now, the depths to the groundwater table are thought to be 2–7 km in equatorial zone and 11–20 km at the poles (Stamenkovic et al., 2021). The contrast of the lighter density of such aquifers, if present, with respect to the heavier Martian basaltic crust makes the MaQuIs gravity mission ideal for detecting and exploring locations and size of possible present-day aquifers or the permeable structures that host them (porous sediments, fractured basalts). The mission could also detect how seasonal and orbital changes of Mars affect the groundwater level on Mars. High precision gravity observations could explore this subsurface phenomenon, which would have important implications for the current habitability of Mars.
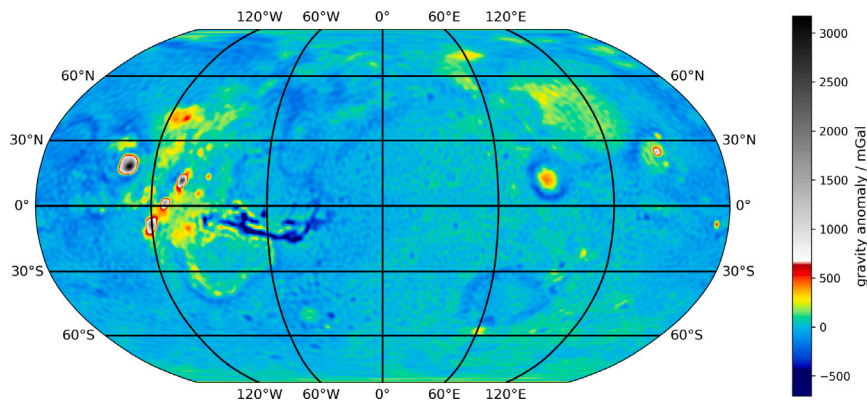
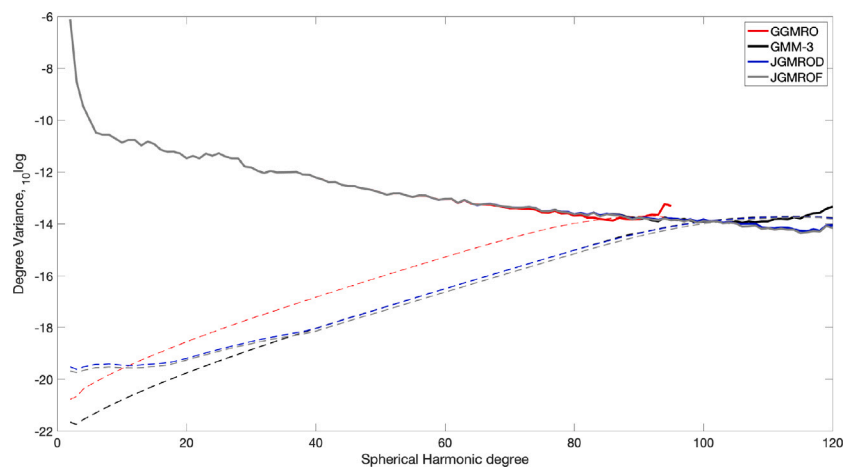**Fig. 1.** Gravity anomaly of Mars from MRO120F (Konopliv et al., 2020).

Fig. 2. Spectral signature of several Mars gravity models found on NASA's Planetary Data System (GGMRO-95 Konopliv et al., 2006, GMM-3-120 Genova et al., 2016, JGMRO-120d Konopliv et al., 2016, and JGMRO-120F models Konopliv et al., 2020).

2.2.2. Volatile-rich subsurface sediments on Mars

One main objective of the proposed mission is the identification and quantification of volatile-rich sediment reservoirs. Numerous landforms on Mars have been interpreted as mud volcanoes and corresponding mud flows, i.e. the results of subsurface sediment mobilization and subsequent ascent, eruption and surface emplacement of volatile-rich, liquefied sediments (Skinner and Tanaka, 2007; Oehler and Allen, 2010; Komatsu et al., 2016; Brož et al., 2019; Orgel et al., 2019; Cuřín et al., 2023). Such deposits are prime targets for geological research, as they bear a record of aqueous processes at depth and are not heavily affected by high-temperature and high-pressure alteration (unlike impact ejecta). As such, they enable access to materials that were formed in the early history of Mars. Moreover, mud volcanoes would be promising sites to search for biosignatures, as mud volcanoes on Earth are known to be habitats for thriving bacterial communities (Fryer et al., 2020) and, by analogy, may have provided suitable conditions for life on Mars (Oehler et al., 2021). However, the interpretation of landforms is typically not unambiguous, and at least part of the hypothesized mud volcanoes may also have been formed as 'true', igneous volcanoes. It is therefore essential to test the mud volcano hypothesis by identifying subsurface reservoirs of volatile-rich sediments. On Earth, mud volcanoes are typically associated with density anomalies (Nettleton, 1979; Doo et al., 2015), and gravity surveys are routinely used to characterize sedimentary basins which typically display negative gravity anomalies (Bott, 1960). The contrast between less dense sediments and the denser basaltic and other magmatic rocks that constitute the bulk of the crust will enable MaQuIs to identify sediment subsurface reservoirs and quantify their masses. A comparison of derived gravity maps with

the distribution of possible mud volcanoes will inform our search for deep volatiles and possible habitable subsurface niches on Mars ('deep biosphere', e. g. Michalski et al., 2013).

2.3. Temporal gravity changes and seasonal behaviour of CO_2 ice

The climate of planets are subject to changes in time due to several causes including astronomical forcing (variations of orbital elements), atmospheric escape or out-gassing following natural events. The stability of present day Mars climate and the secular changes are crucial to understand its long term dynamics (Haberle and Kahre, 2010) Analysis has shown that Mars possibly once harboured liquid water on the surface and had a denser atmosphere (Nazari-Sharabian et al., 2020). This combination renders it possible that there once were life forms roaming its surface. Those factors allow to infer a climate collapse taking place in Mars' history. Understanding the processes that led to that event and the still ongoing seasonal changes including the appearance of surface carbon-dioxide ice, render Mars a relevant subject to predicting Earth's future. To gain a complete picture of the underlying processes, internal as well as surface structures and deposition dynamics are important to study.

In addition, the dynamics of the Martian surface, especially with respect to the seasonal sublimation and deposition of Mars atmospheric carbon-dioxide, should be studied intensely as that will give insight in the viscosity structure of the mantle. Mars is continuously subjected to surface loading induced by seasonal mass changes in the atmosphere and ice caps due to the CO_2 sublimation and condensation process. It results in surface deformations and in time variations of gravity.

Time variations of gravity are not only due to mass variations in surface fluid layers but also to surface loading deformations of the solid component of the planet induced by them (Karatekin et al., 2011). With about one third of Mars' atmosphere being deposited and sublimated in those seasonal changes, the impact on its gravitational field and rotation are immediately recognizable (Karatekin et al., 2006b). The deformations of the planet depend on its internal structure, particularly on its density and elastic parameters. The effect of the internal structure of Mars on its loading deformation is determined via Mars' load Love numbers which depend strongly on the mean radial structure. Low degree load Love numbers (inferior to degree 10) depend essentially on the radius of the core and on its rheological properties (Métivier et al., 2008). While the effect has been observed (Konopliv et al., 2011), the dynamics itself and the driving forces are still subject to active research. More precise gravitational field data can aid in the research of these dynamics.

The carbon-dioxide results in permanent ice sheets of a thickness of approximately $2 \, km$ and areas with a diameter of roughly $1000 \, km$ and $400 \, km$ on the Northern and Southern polar caps respectively. The deposited ice sheet is far from smooth and includes steep cliffs and troughs. While some of those patterns can be attributed to rotation, Coriolis forces, and winds, the models currently fall short in explaining all observations. Moreover, precise gravitational field data could shed light on subterranean structures and density distributions, aiding in building more complete models of the polar ice sheets, explaining the occurring shapes.

The largest signature in the seasonal mass exchange between the Mars polar caps is given by variations in the zonal coefficient of Mars. Martian degree 2 and 3 time-variable gravity coefficients have been estimated by different authors using Mars orbiter radio tracking data (e. g. Konopliv et al., 2011; Genova et al., 2016) as well as numerical genera circulation models (Karatekin et al., 2005). The seasonal time variations of gravity are expected to be mostly induced by surface fluid dynamics as show by high correlations of these observations with atmospheric models (Karatekin et al., 2006a).

Sensitivity studies of the orbital tracking based gravity models show that some seasonal gravity signature can be absorbed in the drag model if constraint is too loose (Konopliv et al., 2011). This shows that a dedicated gravity mission would not only result in a more accurate determination of the temporal gravity field, but would also improve atmospheric models of Mars. The J_3 changes are larger and better detectable than the J_2 temporal variations, on average the odd degrees are about 20 percent higher than the even degrees (Konopliv et al., 2011). This signal is linked to the seasonal CO_2 ice mass exchange of the northern and southern poles of Mars (Konopliv et al., 2011). This mass exchange between poles is estimated to be $\pm 4 \times 10^{15}$ kg and consistent between different studies (Konopliv et al., 2006; Smith, 2009; Yoder et al., 2003). More recent, seasonal variation of the J_2, J_3, J_4, and J_5 coefficients have been estimated from orbital tracking (Genova et al., 2016) and show similar trends in the polar mass exchange. The Mars Orbiter Laser Altimeter (MOLA) on the Mars Global Surveyor (MGS) spacecraft, measured seasonal changes in the ice thickness up to 1.5–2 meters due to the carbon dioxide cycle (Smith et al., 2001). The volume of CO_2 and water ice variability is estimated to be 9.4×10^{12} m^3 to 9.6×10^{12} m^3 for the Southern and Northern polar caps based on MOLA measurements (Xiao et al., 2022a,b).

In addition to atmospheric mass transport, tidal deformation of Mars also results in a time-variable gravity signal. Although this signature is substantially larger than that of the atmospheric mass transport, its behaviour is much more predictable and easily quantified. Typically, its influence is parameterized by the k_2 Love number that quantifies time-variability of the degree-two gravity field coefficients.

This Love number is an important independent geodesy constraint (Rivoldini et al., 2011), and helps to constrain the rigidity structure and core size of Mars (Pou et al., 2022). It has been determined in various previous Mars gravity field determinations (Konopliv et al., 2011, 2016;

Genova et al., 2016), where (Genova et al., 2016) shows the strong need for proper modelling of the atmospheric properties to properly extract the signature of the Love number. For the Moon, separate values of k_{20}, k_{21} and k_{22} have been determined using GRAIL data, providing further interior constraints (Williams et al., 2014). Although these values of k_{2m} at different orders m proved to be almost equal to one another, their small differences may be relevant in processing of high-accuracy data proposed here. Past attempts to measure these separate coefficients using Doppler tracking proved unsuccessful for Mars. In addition to the nominal value of the Love number(s), the phase lag of the tidal deformation, often quantified by the k_2/Q value provides constraints on the Martian interior (Pou et al., 2022), and is a crucial parameter for the long-term orbital evolution of the Martian moons (Efroimsky and Lainey, 2007). At present, the Martian k_2/Q at Phobos' forcing frequency is best constraint by the secular acceleration of Phobos' orbit, as determined in its ephemeris (Lainey et al., 2021). Determining the frequency-dependence of k_2/Q could provide further constraints on both Mars interior and system evolution, provided their signature in the data could be decoupled (Dirkx et al., 2014).

Studying the formation of the Tharsis Rise will reveal more information about the planet's interior and its thermal evolution. One big question to solve is if the mantle underneath the Tharsis Rise is still active and taking part in dynamically upholding the volcanic dome. The Insight mission is placed near Elysium Mons, which is in the seismographic shadow zone of the Tharsis Rise and therefore receives less information from that area. However, a dedicated gravimetry mission that would be capable of measuring gravity-rate data could observe if there are changes in the gravity field due to mantle flow. A similar phenomenon on Earth, yet due to another physical process, is observed by GRACE: mantle flow due to Glacial Isostatic Adjustment (Steffen et al., 2009; Root et al., 2016). A prominent feature in the free-air anomaly and in the isostatic anomaly of Mars is a huge gravity signal at the Tharsis Rise with an extreme high at the centre of the dome, surrounded by a negative ring around the region (Zhong and Roberts, 2003). Because it is also visible in the isostatic anomaly it could be interpreted as still active readjustment (Root et al., 2015), meaning mantle plume movement underneath the Tharsis Dome. A preliminary study (Root et al., 2022) of a mantle anomaly underneath the volcanic region, suggests $12 \, \mu Gal \, yr^{-1}$ gravity change for the very long wavelength gravity signal. This will require accurate observations of the secular change of the gravity field, decoupled from any atmospheric interactions.

2.4. Internal structure and composition of Mars

The internal structure of any planetary body, including tectonic lithosphere, core size, mass distribution, and material composition, are an intensely studied field to understand the formation of planets and their current dynamics. This includes phenomena such as volcanic and seismologic activities. To study those on Mars, a seismograph was deployed on Mars' surface (Lognonné et al., 2019) with the Insight mission. By studying the seismographic data from the Insight mission, new insights were obtained into the inner composition and structure of the planet and they have given new constraints in lithospheric and mantle dynamic modelling. Based on determination of the polar moment of inertia, the tidal varying potential and seismic data from the Insight mission the Martian core radius was determined as $1830(40) \, km$ (Stähler et al., 2021). The corresponding core density ranges between $5800 \, kg \, m^{-3}$ to $6200 \, kg \, m^{-3}$ showing substantial amounts of volatiles contained in the core when compared to a pure iron density of about 8000 kg/m^3. From the lack of S-waves in the seismic record a fluid state of the core is derived. At the Insight landing site a crustal thickness of $39(8) \, km$ was derived from seismic data (Knapmeyer-Endrun et al., 2021) which fits to global estimates of crustal thickness from gravity and topography data of $27 \, km$ to $89 \, km$ (Neumann et al., 2004). The expected crustal thickness variations

depend on the assumed structure with possibilities of (a) a homogeneous crustal density, (b) an upper porous layer and more compact material in the lower part of the crust and (c) a possible dichotomy between northern and southern part of the crust (Wieczorek et al., 2022).

Complementary to seismic data, the gravitational field distribution can be used to improve our understanding of the inner structure. With the current gravity field models obtained by tracking the orbital spacecraft, the global resolution of the Martian gravity fields is known up to wavelengths of approximately 115 km (90 d/o) (Konopliv et al., 2011; Genova et al., 2016). Due to the elliptical orbits of the tracked spacecraft there remain asymmetries in the resolution of the gravity field with respect to northern and southern latitudes.

On Mars two global surface features stand out that are a result of the internal dynamics of Mars: the crustal dichotomy and the Tharsis Rise, a huge volcanic province harbouring the largest volcano in the Solar system. Both structures are heavily debated about the time of formation, but the mechanism of formation is usually described by mantle plume volcanism (Zhong et al., 2007). A huge up welling penetrated the primarily crust during the Early Noachian depositing the rock mass that are now the southern highlands. Then, in the Late Noachian another plume eruption is responsible for the creation of the Tharsis Rise. This early creation of the Tharsis Rise is now debated (Bouley et al., 2016), because a later formation could have caused sufficient polar wander to explain the orientation of Noachian/Early Hesperian valley networks around the equator, suggesting a different orientation of Mars in more humid climate. Even the northern planes in this model lacks the heavily cratered landscape that would prove its old age. The northern planes are quite smooth and show less signs of heavy cratering. However, the old surface could have been overprinted as a number of buried impact basins, called Quasi-Circular Depressions (QCD), were discovered that indicate the old age of the northern region (Frey et al., 2002). These QCDs are visible in the Mars Orbiter Laser Altimeter data, but do not have an imagery signature. High-resolution gravity observations could confirm the presence of buried impact structures.

Combining topographic (Klimczak et al., 2018) and gravity data (Zuber et al., 2000; Beuthe et al., 2012; Goossens et al., 2017) it is possible to study the structure of the martian lithosphere. Flexure theory (Watts and Burov, 2003) is able to compute characteristics of the lithosphere by studying the spectral interplay between topography and gravity. For example, Phillips et al. (2001) show that flexural lithosphere loading is the main support of Tharsis for example, following the initial studies by Turcotte et al. (1981). A long standing research has been performed to estimate the elastic thickness on Mars, which controls the amount of support of which the lithosphere is capable, which is extreme on Mars. The Tharsis region, one of the largest volcanic complexes in the Solar system, has been thoroughly studied (Belleguic et al., 2005; Beuthe et al., 2012; Lowry and Zhong, 2003; McKenzie et al., 2002). One drawback of this theory is buried mass anomalies that do not have any topographical signature (McKenzie et al., 2002). Inspection of the Bouguer anomaly of the Northern Hemisphere of Mars shows clear evidence of numerous sub-surface mass structures (Zuber et al., 2000). These structures are not only subsurface aquifers, but the northern hemisphere has many buried impact craters (QCD) that are indications of an Early-Noachian age, maybe going back to the primordial crust, now overprinted by southern erosion deposits (Frey et al., 2002). A recent flexure study by Root and Qin (2022) shows higher global density, confirming high basaltic crust. Thin shell flexure is able to explain part of the long-wavelength features, but dynamic flow is needed, and high lateral densities are present in the martian crust, as homogeneous models cannot represent the gravity field completely. The need for lateral varying crustal density observations is needed to better understand the geological past of Mars and its current state.

With gravity alone, it is difficult to determine the depth of these structures, whether they are present in the crust of upper mantle. Earth-based gravimetric studies (Bouman et al., 2013; Root et al.,

2021) show that gravity gradients are more sensitive to crustal mass anomalies and are better capable of decoupling them from any upper mantle mass anomalies. Global inversion modelling together with state-of-the-art flexural modelling show promising results in determining crustal and upper mantle mass anomalies, when using gravity gradient data (van Brummen, 2022). Global coverage of the gravitational field measurement allows for modelling of the entire planet and enable the study of large scale dynamics and high mass erosion or deposition. Additionally, global data supplemented by local data and imagery can improve models and allow more precise predictions of local static and dynamical behaviour. The latter is especially important to identify specific regions that show distinct different variations in the density structures of the crust.

Additional information can be gained from sounding radar missions (Heggy et al., 2001; Seu et al., 2007) potentially penetrating the ground several hundred meters. Due to absorption and reflection of the radar signals, these missions excel especially in shallow-depth investigations of the planet and are mainly deployed to investigate surface effects (Smirnov et al., 2014).

To gain a complete picture of the composition and dynamics of Mars, the different measurements need to be combined. The gravitational data delivers an additional level to the existing data, which cannot be addressed by other means and vice versa. Existing image and MOLA data as well as new laser altimetry data, potentially collected in the scope of MaQuIs, providing the topography combined with upper soil layers from radar observations add constraints to the gravity field solution. This allows for an increase in d/o compared to the standalone satellite gravimetry solution.

2.5. Scientific requirements

For this scientific overview we identified the following requirements for a dedicated gravity field mission to Mars.

- Spatial resolution: The resolution of the gravitational field shall be improved above the spherical harmonic (SH) degree 90 (approximately 115 km) for better flexural modelling of the Martian Lithosphere. For improved mapping of crustal structures, the mission should aim for a global gravity field resolution up to 360 d/o.
- Minimum size aquifers: Mapping the crater size aquifers requires a resolution of 2880 degree and order spherical harmonic coefficients to detect. The Lunar gravity field's best resolution is in the order of 1200 d/o (Lemoine et al., 2013). As it is discussed, the Martian system already greatly benefits from an improvement of the current resolution which is up to the order of 90–100 degree and order. Larger aquifer volumes, such as that which created the Valley Marineris, can be mapped with a gravity field up to 360 degree and order.
- Quasi-Circular Depression (QCD) determination: MaQuIs shall improve the understanding of the formation of the dichotomy of Mars by determining the age of the northern hemisphere (Frey et al., 2002). If the QCD are identified as craters, this could change the age determination (by crater counting) of the northern hemisphere significantly.
- Global Coverage: Polar regions (ice sheets) are situated poleward above 80° latitude north and below 80° latitude south. MaQuIs shall cover that range to support glacial isostatic adjustment and Martian climate studies. This results in a requirement for a nearly polar orbit.
- Temporal frequency seasonal: The sub-yearly signal in $C_{30} = \pm 5 \times 10^{-9}$ and $C_{50} = \pm 3 \times 10^{-9}$ (Smith, 2009). The corresponding mass changes are in the north pole $2(2) \times 10^{15}$ kg, south pole $3(4) \times 10^{15}$ kg, atmosphere $-4(2) \times 10^{15}$ kg respectively. MaQuIs shall be able to address these changes.
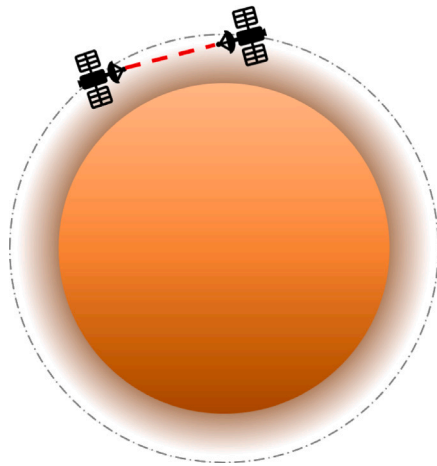
Fig. 3. A sketch to show the measurement principle: Two satellites chasing one-another along the same orbit to measure changes in the gravitational field by detecting the change in the distance between the satellites.

- Temporal secular: Based on preliminary modelling mantle convection underneath the Tharsis region could come up to $12\,\mu\text{Gal}\,\text{yr}^{-1}$ (Root et al., 2022). As such, the secular drift in the Odyssey $\bar{J}_3$ data is limited to $0.9(9) \times 10^{-11}\,\text{yr}^{-1}$ (Konopliv et al., 2011). By observing this effect, which is already at the detect-ability of the current gravity field estimates, with a dedicated gravity instrument, MaQuIs would be able to better constrain the viscosity structure of Mars and prove that that ongoing mantle dynamics are present on Mars. We propose that MaQuIs should be designed to be able to observe 0.01 microGal per year global changes of the gravity field to have significant science return.

2.6. Proposed mission

Fig. 3, outlines the overall scheme of the measurement principle. The MaQuIs mission consists of two satellites chasing one another along the orbit to map the gravitational field of Mars.

MaQuIs follows missions such as the Gravity field and steady-state Ocean Circulation Explorer (Rummel et al., 2011), the Gravity Recovery And Climate Experiment and its Follow-On mission (Tapley et al., 2004; Kayali et al., 2017), designed to detect static and dynamical processes on Earth, as well as the Gravity Recovery and Interior Laboratory (Zuber et al., 2013), a GRACE like mission orbiting the Moon. Those missions, have successfully demonstrated that the outlined scientific goals are achievable by deploying gravity missions in orbit.

The requirements towards MaQuIs to fulfil the outlined scientific goals are discussed in this paper. The following sections will give reasons and context for achievable sensitivities and involved challenges.

2.7. Pathfinder

In addition to the mapping of Mars, MaQuIs can serve as a pathfinder mission for future quantum-based gravity field missions. With the technology from MaQuIs, miniaturizing systems and preparing them for reliable operation in deep space, missions to map the gravitational field of different planetary bodies become more and more available. Especially the possibility to measure dynamics of subterranean oceans renders such experiments interesting for future mission to the moons of the gas giants. With appropriate correction of drag, this could also be envisaged to measure the gravitational field of the gas giants themselves.

Other areas of interest, for which MaQuIs could be a pathfinder, are comparative planetology and the study of climate change on other planets and on Earth. For the latter, systems are currently developed, which share a lot of synergy with MaQuIs.

As the name suggests, MaQuIs will make use of quantum technologies to achieve the planned accuracy. In this case, especially cold atom sensors are foreseen in combination with optomechanical inertial sensors and stabilized laser links. With those technologies in place, MaQuIs can act both as a pathfinder for future quantum technologies deployed in space and as a technology driver to develop the necessary setups. The recently developed cold atom roadmap (Alonso et al., 2022) and the summary of quantum physics in space (Belenchia et al., 2022) detail current and planned activities in the area of quantum technologies in space.

2.8. Summary of the scientific goals

The scientific goals of the mission can be summarized as follows. MaQuIs shall:

- Improve the gravitational field map of Mars
- Detect subsurface structures, especially water occurrences and buried impact craters
- Improve the knowledge of the internal structure of the planet, both crustal and mantle structures
- Determine if current mantle convective processes can be observed
- Monitor seasonal changes on the surface
- Aid in understanding the climate collapse and its comparison to dynamics on Earth
- Measure planetary dynamics and subsurface changes
- Identify areas of increased and decreased density
- Inform future landing sites
- Act as a pathfinder for future quantum-based missions, especially to other celestial bodies

3. Detection requirements

3.1. Expected signals

The static gravity field (gravity anomaly: gravity minus gravity of reference ellipsoid) of Mars ranges from $-695\,\text{mGal}$ to $3135\,\text{mGal}$ (Konopliv et al., 2016). The majority of the gravity anomalies do not exceed $\pm 500\,\text{mGal}$ and only the major volcanic regions result in higher gravity anomalies (see also Fig. 1). The order of magnitude, excluding these volcanic areas, is comparable to the Earth's gravity field of about $-300\,\text{mGal}$ to $470\,\text{mGal}$ (Zingerle et al., 2020).

The temporal gravity field variations seem to be dominated by CO_2 exchange between the northern and southern hemisphere and the tidal potential from the Martian moons, Phobos and Deimos. For the mass changes at the poles between Summer and Winter given in Section 2.3 the gravity signal at an orbit height of $150\,\text{km}$ to $200\,\text{km}$ is in the order of $230\,\mu\text{Gal}$ using a disc shaped mass distribution and a spherical approximation of Mars.

3.2. Noise sources

For the mission under consideration, the atmospheric drag will be the main disturbing force. It depends strongly on the spacecraft geometry, the velocity of the spacecraft and the atmospheric density, which increases with decreasing orbital altitude. It is difficult to numerically assess it with a high precision. General Circulation Models (GCMs) and ionosphere-thermosphere models are commonly used to model the atmosphere on large scales, as for example the longitudinal dependence of the atmospheric density and its annual changes. But they fail to capture the short term variations in the Martian upper atmosphere, as has been confirmed during operational aero-breaking maneuvers by many previous space missions from ESA and NASA (e. g. Castellini et al., 2018).

Typically, mis-modelling of atmospheric density is accounted for in the determination of planetary gravity fields from Doppler data by the estimation of correction terms, such as drag scale factors and empirical accelerations (Genova et al., 2016). For spacecraft equipped with high-accuracy accelerometers, such as the ESA missions BepiColombo to Mercury and the Jupiter Icy Moons Explorer (JUICE), these effects can be directly measured, significantly reducing the potential noise on the gravity field solution induced by these effects (Cappuccio et al., 2020).

Recently, accelerometers on board the Mars Atmosphere and Volatile Evolution (MAVEN) spacecraft have monitored the neutral density in Mars thermosphere (above approximately 120 km). This region affected by radiation and energy deposition from the Sun and by energy and momentum from the lower atmosphere orbit-to-orbit variability is found to be still significant (Zurek et al., 2017).

For a low altitude flying mission like MaQuIs atmospheric drag will be as significant as it is the case for the MAVEN. Onboard precise accelerometers and inertial measurement units (IMU), similar to those onboard MAVEN, can measure directly the net acceleration, determine its effect on the orbit and correct for. In addition, these measurements allow for a better determination of Martian atmospheric properties, which will improve the tracking data analysis of other missions. Atmospheric density measurements along the orbiter path would yield hydrostatic density and temperature profiles, along track and latitudinal density waves, and latitudinal and longitudinal density variations (Zurek et al., 2017). Moreover, the surface loading variability due to atmospheric mass transport will have a measurable influence on the Martian gravity field, making knowledge of the Martian atmospheric dynamics directly relevant for interpreting measured temporal gravity change.

In addition to non-gravitational noise sources the gravitational effects of Phobos and Deimos with semi-major axes of the respective orbits of 9376 km and 23 463 km have to be taken into account having a major influence on a spacecraft. For a mission like Mars Global Surveyor, with an orbital height around 400 km, the gravitational effect is larger than atmospheric drag (Konopliv et al., 2006). The masses and orbits of Phobos and Deimos are therefore estimated in the gravity field recovery process. Unlike atmospheric density, the dynamics of the Martian moons is well constrained and its evolution is predictable (Lainey et al., 2021), and with proper model consideration, this influence will not pollute the gravity recovery.

The determination of the Martian gravity field is typically done concurrently with the determination of its rotational parameters. The relationship between rotation (i.e. mainly Length-of-Day but also Polar motion) and time-variable low degree gravity coefficients has been well established (Karatekin et al., 2006b, 2011). Their determination from single orbiter tracking can be challenging, partly due to the sensitivity of zonal harmonics to orbiter geometry but also because of the low-degree zonals obtained from a single orbiter tracking analysis are contaminated by higher-degree harmonics with non-negligible seasonal variations. For the proposed mission, insufficiently accurate determination of the Mars Orientation Parameters (MOPs) could lead to unmodelled rotational variations being interpreted as temporal gravity field variations at the same frequency. For terrestrial and lunar gravity field determination, this is mitigated by geodetic techniques and LLR, respectively. For Mars, the use of lander tracking data (such as InSight) will be important (Kuchynka et al., 2014; Folkner et al., 2018), since these data are sensitive only to rotational variations and not temporal gravity changes.

3.3. Link pointing requirements

The Laser Ranging Interferometer (LRI) on-board GRACE-FO requires a pointing accuracy of the laser beams with respect to each other of less than 100 µrad (Abich et al., 2019). This requirement is driven by the amount of received laser power and by the required level of angular overlap of the beams in order to produce a detectable interferometric
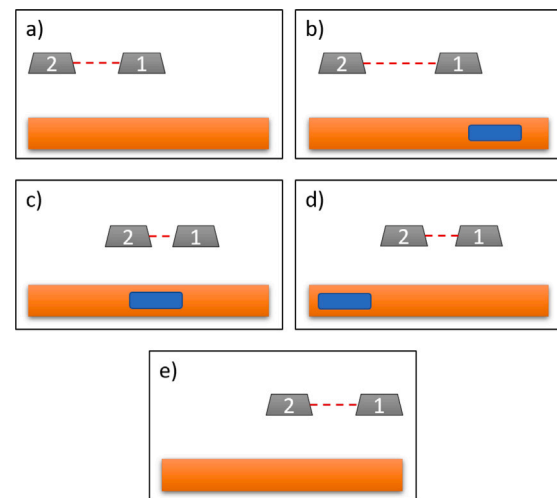

Fig. 4. A sketch to show the measurement principle: Two satellites chasing one-another to measure changes in the gravitational field due to the change in the distance between the satellites. In this sketch it is shown how satellite 2 chases satellite 1 (tabloid a)). If the underground is denser, here represented by the blue rectangle, the first satellite is accelerated by the resulting increased gravitational force (tabloid b)). Once satellite 1 passes that dense portion, it is decelerated, while satellite 2 feels the attractive force. The distance between the two satellites is reduced (c)). With the deceleration of satellite 2 passing (d)), the original distance is re-established (e)). From the variation in distance, the gravitational field is determined.

beat note signal. This has two consequences: (1) A beam steering mechanism is required to maintain proper beam pointing between the satellites. This is necessary due to larger orbital variations than 100 µrad and performance limits of state-of-the-art spacecraft attitude and orbit control systems. The mechanism developed for GRACE-FO has demonstrated a pointing error below 10 µrad on ground (Schütze et al., 2014).(2) A link acquisition procedure, potentially including the use of dedicated hardware (see Section 4.5.1), needs to be foreseen that ensures the sufficient pointing of the laser beams on the two spacecraft prior to the instrument's transition into science mode (Koch et al., 2018; Koch, 2020).

4. Proposed mission scenario

4.1. Mission summary

MaQuIs is proposed as a gravity field mission. It follows the configuration of GRAIL (Zuber et al., 2013), GRACE (Tapley et al., 2004) and GRACE-FO (Abich et al., 2019) and consequently consists of two satellites trailing each other, as shown in Figs. 3 and 5. The two satellites are connected by an optical link.

If one is subjected to an increased gravitational field, e. g. caused by a denser material on or below the Martian surface, it is accelerated. The acceleration then leads to a variation of the distance between the two satellites which can be translated into a gravitational signal. This process is sketched in Fig. 4.

The accuracy of the ensuing measurement depends on the stability of the optical link, the correction for drag and other non-gravitational accelerations acting on the satellites, the orbital velocity, and the distance to the target body.

4.2. Terrestrial and Lunar experiments

Global gravity missions, mapping the field distribution have been deployed to observe and investigate Earth (Rummel et al., 2011; Tapley et al., 2004). These missions were determined to study, among other goals, the effects of climate change by monitoring sea level rise and

Fig. 5. Artist's impression of a gravity mission consisting of two spacecraft in a low-Earth orbit deploying an optical intersatellite laser link (credit DLR-SI).

oceanic dynamics through gravity field observation (Tapley et al., 2019).

The results of these missions combined with images of the Earth allow for determination of density distribution on Earth and foster understanding of our planet and its inner structure (Mandea et al., 2020).

Additionally, future missions to map the gravity field of the Earth are investigated (Haagmans et al., 2020) to meet the end user demands of gravity field products (Pail et al., 2015). The next generation of gravity measurements from orbit is set to include quantum sensors as inertial measurement units. Several such missions have been proposed. The next steps in quantum sensor development for setups based on cold atoms is, for instance, outlined by Alonso et al. (2022).

Similarly, GRAIL (Zuber et al., 2013), was deployed to understand the inner structure and density distribution of the Moon (Goossens et al., 2020). While GRAIL did not deploy quantum sensors in its design, it successfully demonstrated that a gravimeter mission is the desired tool to investigate celestial bodies in greater detail and higher precision.

4.3. Flight configuration & orbital considerations

MaQuIS will be composed of two satellites trailing each other at a distance of at least $200\,\mathrm{km}$. The distance will be monitored by a bi-directional optical link between the satellites. Star tracker and communication to Earth will ensure tracking of the orbital parameter and thruster on board both satellites will enable corrections.

MaQuIS will be in an areocentric orbit altering the relative inclination due to the rotation of the planet, scanning the entire planet over time. If, however, it becomes apparent, that a specific region or that the dynamics of a specific region, such as the polar ice caps during sublimation of the CO_2, are of increased interest, this plan could be changed in favour of an uni-planar orbit.

The achievable accuracy of the measurement is determined by several factors, two of which are linked to orbital considerations:

1. Orbital Height
   The orbital height impacts the measurement directly, as the closer to the surface the two satellites fly, the more pronounced is the effect of the gravity field variations, which can be observed by the instruments on board the spacecrafts. For comparison, GRAIL orbited the Moon in a lowest altitude of $30\,\mathrm{km}$, while GRACE orbited Earth in an altitude of $\approx 450\,\mathrm{km}$.

2. Atmospheric Density
   In general, the atmospheric density, and thereby the drag is lower the further an orbiting satellite is dispatched from the planet. With increasing atmospheric density, two effects have to be considered:

   - vibrational noise due to the interaction of non-gravitational accelerations and (deployable) structural elements, and

- limitations on the mission life time due to deceleration of the satellites.

In order to achieve the targeted sensitivity a trade-off has to be made between the orbital height and the acceptable atmospheric drag. On ground level Mars' atmospheric density is only $6\,\mathrm{hPa}$, about 0.6% of Earth's atmospheric density. However, the density does not decrease with altitude as rapidly as is the case for Earth. Hence, an orbit higher than that of GRAIL above the Moon but lower than that of GRACE above the Earth can be chosen for MaQuIS with respect to Mars. Flying at a lower altitude allows for a better determination of the gravity field, both in terms of degree strength and uncertainty. However, the influence of atmospheric drag increases with lower altitude, which requires a more propellant and/or a different orbit control system (such as continuous low thrust) to maintain the orbit for a sufficient amount of time. At an altitude of 170 km, the mean atmospheric density is roughly similar to that experienced by the GOCE spacecraft at Earth, on the order of 10^{-11} kg/m^3. At 200 km and 250 km, it is on average one and two orders of magnitude smaller, respectively, while at 100 km it is three orders of magnitude larger than for GOCE. This trade off will depend on the ballistic coefficient of the satellites, the mass and power budget available for the propulsion system, requirements on static and temporal gravity field determination quality, variability of the Martian atmospheric density, risk trade-offs, the possibility to eliminate the use of deployable structures, etc. A comprehensive system study should be performed to trade off these various aspects.

Other contributing noise factors, also those stemming from orbital choices, are summarized in the following chapters as well as the targeted sensitivity.

4.4. Target sensitivity

As it is discussed above, the subsurface lakes are in the order of $10\,\mathrm{km}$ in diameter. The surface ice sheets have been measured to be in the order of several hundreds to thousand kilometers in diameter with thickness in the order of several kilometer.

While other scientific goals have been determined, the detection of the subsurface water reservoirs is the central scientific goal. It simultaneously is the most challenging. The detection of the subsurface water reservoirs does not only depend on their diameter, but mainly on their volume. To resolve the currently discussed occurrences, a spatial resolution for static measurements on ground in the order of several tens of kilometers is targeted by MaQuIS. In case of static measurements, averaging over several measurements and orbits, and thereby periods of time, is possible and increases sensitivity. The resolution for dynamical processes can be relaxed, since those target primarily the sublimation and deposition of large amounts of CO_2 on the poles.

There is a trade-off between the orbital height and the duration of the mission. The first parameter is driving the maximum resolution of the observed gravity field, when flying lower the satellite pair will be more sensitive to the high d/o signals of the static gravity field. The drawback of flying low is the increased atmospheric drag on the satellites, resulting in a faster de-orbiting, when no drag-free control system is taken onboard. However, for an optimal observation of the time varying gravity signal, a longer mission duration is necessary. A full trade-off analysis is needed in a CDF study, but some qualitative estimates for the static gravity field resolution can be obtained by the error covariance values of Bills and Ermakov (2019).

The satellite-to-satellite tracking formula is used (equation 25 and 26 in Bills and Ermakov (2019)). This calculates the estimated error for a satellite pair with a certain link in between. Fig. 6 shows the estimates errors for different orbital height of a satellite pair (red line).

For these estimates 365 days of data was used using a 10 s integration time with a conservative optical link error of 10^{-8} m/s. Furthermore, we use a pair distance between 0.5 and 2 degrees to mitigate the resonance effect of the observation for certain d/o of the
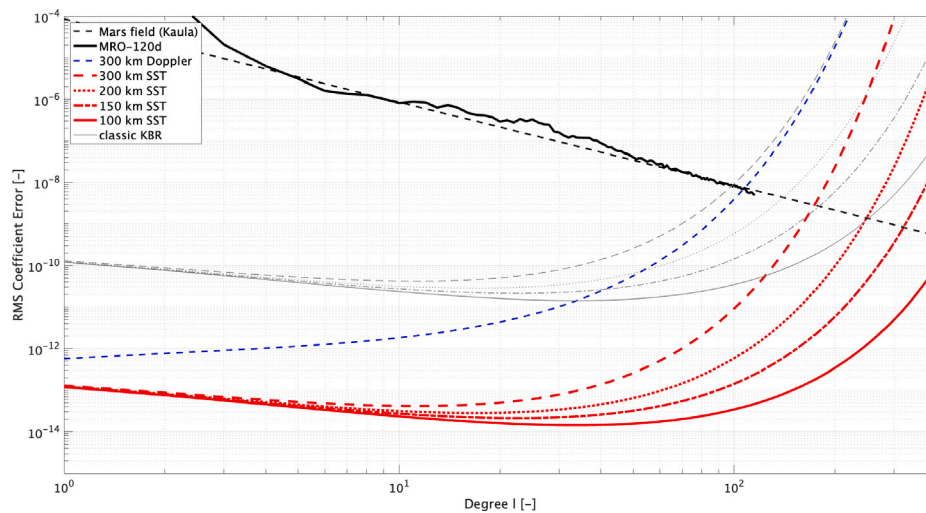
Fig. 6. Error estimates of gravity missions around Mars for different orbital height. The blue dashed line is the estimate for a Doppler-based mission at 300 km. The SST mission with optical link is shown in the multiple red lines and for a classic KBR-based error estimate is shown in grey lines. The signal RMS related to the observed gravity model MRO_120d (Konopliv et al., 2011) and a fitted Kaula power law ($8.5e-5/l^2$) for the higher degrees are shown in black.

gravity field. The error estimates are related to the static gravity field model MRO_120d (Konopliv et al., 2011) together with a Kaula power law ($8.5e-5/l^2$) for the higher degree. The Doppler estimate (dashed blue) was made to calibrate the equations and resembles the estimates from Bills and Ermakov (2019). The satellite-to-satellite tracking estimates show the high performance of the optical link. For the similar orbital altitude as for the Doppler data, the SST mission would increase the gravity field estimate to almost 200 d/o. By lowering the orbit height the resolution would increase to around 360 d/o for an orbital altitude between 100 and 150 km. This low height could be obtained at later stage of the mission. The laser link really competes with the classical KBR, because of the superior precision of the optical link.

4.5. Payload design

4.5.1. Primary instrument

As was the case for both the GRACE and GRACE-FO missions, the two satellites are equipped with the same systems. Fig. 7 outlines the primary instrument design, without any redundancy measures. The figure schematically illustrates the combination of a laser interferometer ((a)–(e)) and a hybrid quantum sensor ((g) and (f)). Thereby, the laser interferometer is sketched as an off-axis design, building on the layout of the successful LRI. At a later stage it will have to be evaluated whether an off-axis or an on-axis design (where the received and transmitted laser beams share a common optical path) is advantageous in the context of the overall mission. For this, the required level of redundancy, the inter-satellite distance and other parameters will have to be taken into account. The optical link is received at entry point (c) from which it travels to the optical bench at (d). There the interference signal between the received beam and the locally generated beam (e) is obtained. The link then proceeds to the beam routing optics at (a), which are surveyed by a combination of the optomechanical inertial measurement unit (f) and the atom interferometer (g). Eventually, the light is transmitted to the other spacecraft via the exit pupil at (b). The other satellite includes the same setup and is mirrored with respect to the first satellite. In the following, the systems are explained individually.

The sketch also shows the acceleration of the satellite $\vec{a}$ along the shown axis. Accelerations along other axes, as well as rotation, have to be treated equivalently. The following paragraphs describe the components that make up the primary instrument:

Laser Ranging: Both spacecrafts share an interferometric bidirectional laser link to measure relative changes in the distance between the
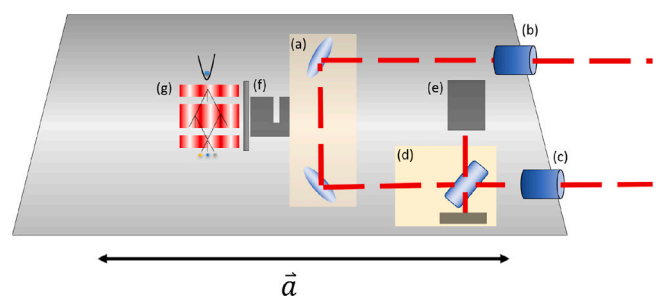

Fig. 7. This sketch outlines the primary instrument. It consists of the laser link between the two satellites, which comes in at point (c), is then combined with the signal of the stabilized internal laser (e) on an optical bench (d), where the beat between the two signals is measured. The laser beam is then guided towards the exit aperture (b) via the beam routing optics at (a), which are situated as close to the centre of mass of the spacecraft as possible to reduce residual accelerations. The beam routing optics are surveyed by a combination of quantum accelerometers (optomechanical inertial measurement unit, OMIS (f) and the cold atom interferometer (g). Finally, the laser signal is send to the other satellite through (b), where the system is mirrored.
The vector $\vec{a}$ shows the acceleration of the satellite due to, for instance, atmospheric noise.
The sketch shows one dimension, the other dimensions have to be treated separately.

two satellites. This distance measurement depends on the chosen laser wavelength. For this mission, a wavelength in the infrared (1064 nm to 1550 nm) is envisioned due to flight heritage and the availability of well-suited components, e.g. optics, lasers and resonators. As stated previously, both spacecrafts host identical hardware. For the purpose of laser ranging this includes: lasers (Bachman et al., 2017), optical benches (Abich et al., 2019; Dahl et al., 2016), potentially retroreflectors (Dahl et al., 2016), instrument control (Bachman et al., 2017) and laser frequency reference units (Thompson et al., 2011; Sanjuan et al., 2019).

Space proven interferometric link technologies and laser modules exist and have been developed for several different applications, including deep space missions such as LISA (Antonucci et al., 2012). The Laser Ranging Interferometer of the satellite gravimetry mission GRACE-FO, successfully operating since 2018, reaches a noise level of about $10\,nm/\sqrt{Hz}$ at $40\,mHz$ and about $300\,pm/\sqrt{Hz}$ at $1\,Hz$ (Abich et al., 2019). For frequencies below $30\,mHz$ gravity dominates the ranging signal and it is not possible to directly evaluate the interferometer noise floor. However, thorough modelling of the LRI and comparison with GRACE-FO microwave ranging data suggests that the

well-understood tilt-to-length coupling effect, which can be subtracted in post-processing, and laser frequency noise remain the LRI's limiting noise sources in the μHz–mHz frequency range (Müller et al., 2022).

As laser frequency noise is the dominant noise source for a laser interferometer with such unequal arm lengths as is proposed here, the laser frequency must be actively stabilized. Thereby, two distinct timescales are of importance: short timescales between $10\,\mathrm{s}$ to $1000\,\mathrm{s}$, on which the local gravity field underneath the spacecraft is sampled, and timescales of months and years which are important for the tracking of long-term changes of the local gravity field. For the stability requirement on the shorter timescales an optical cavity with optional thermal shielding appears to be the prime candidate (Sanjuan et al., 2019). The longer timescales requirement could be met by minimally invasive measures to the experimental setup to further enhance the stability of these optical cavities. Applicable techniques are currently under investigation in the context of the next generation of Earth gravity field missions (Rees et al., 2021, 2022).

One of the most critical steps in the commissioning phase of an inter-satellite laser interferometer is the initial establishment of the laser link (Koch et al., 2018). In order for the interferometer to function properly the laser beams that are transmitted by both spacecraft have to be aligned to each other with a maximum error on the order of about $\pm 100\,\mu\mathrm{rad}$. Additionally, the frequencies of the involved lasers must match to within the photo-receiver bandwidth of $\leq 37\,\mathrm{MHz}$ (Fernández Barranco et al., 2018). Ground-to-orbit effects, bias angles between interferometer sub-units and other systems on the platform (e.g. star trackers) caused by mechanical tolerances during integration of the units as well as thermally-induced deformations of the spacecraft are the main drivers for a knowledge error regarding the true line of sight between two spacecraft. Hence, an alignment of the laser beams by means of dead reckoning will most probably not be successful. In the absence of absolute laser frequency references also the laser frequency difference of the involved lasers would not match to within the required level due to temperature differences of the different spacecraft and corresponding effects on the lasers and cavities. An appropriate procedure to calibrate this 5-dimensional uncertainty space (two angles per spacecraft and the laser difference frequency) should foresee a dedicated link acquisition system (LAS) on each spacecraft (Koch, 2020). These may include dedicated acquisition light sources that are specifically tuned to the needs of this critical mission phase and sensors that are designed to perform an incoherent detection of any incoming signal. A LAS thus drastically reduces the complexity of the associated link acquisition procedure and can provide a major positive impact to the risk reduction scheme. Especially for a remote mission which orbits another celestial body the latter point is quite significant.

While the components briefly described above define a baseline laser interferometer configuration, different technology options should be considered:

In addition to the stability of the laser frequency, which can be realized by using optical cavities, its absolute value is also of interest as the ranging measurement directly scales with it. Hence, an additional absolute frequency reference, e.g. an iodine cell, could be incorporated (Döringshoff et al., 2017).

In the absence of sophisticated GNSS navigation, a measurement of the inter-satellite distance by using the interferometric laser link seems beneficial. In the context of the LISA mission this technique was developed and tested on ground (Sutton et al., 2010; Heinzel et al., 2011). With only minor additional hardware absolute distance measurements between two spacecrafts below $0.4\,\mathrm{m}$ were achieved with an update rate on the order of a few Hertz (Sutton et al., 2010; Heinzel et al., 2011).

Using the same additional hardware, rudimentary communication protocols can be implemented using the interferometric laser link. On-ground experiments showed the functionality with data rates of up to 20 kbps (Sutton et al., 2010; Heinzel et al., 2011). This technique seems especially compelling as it can be used to transfer data between the

spacecraft and only have one of the satellites communicate with Earth. This measure saves energy and underscores the inherent redundancy scheme that is realized by implementing two identical spacecraft.

Inertial Measurement Unit: Non-gravitational acceleration, e.g. due to atmospheric drag or solar radiation pressure, can obscure the results obtained by the laser link (Kornfeld et al., 2019; Tapley et al., 2004). Additional accelerometers onboard of the satellites enable the reduction of spurious accelerations (Kornfeld et al., 2019; Christophe et al., 2015; Tapley et al., 2004). Current approaches rely on electrostatic accelerometers, that suffer from drifts at low frequencies (Zahzam et al., 2022; Klinger and Mayer-Gürr, 2016; Carraz et al., 2014; Touboul et al., 2012). In this context, atom interferometers (AI) were proposed to replace (Lévèque et al., 2021; Migliaccio et al., 2019; Trimeche et al., 2019; Chiow et al., 2015) or complement the classical accelerometers (Zahzam et al., 2022). By principle, atom interferometers can provide absolute and long-term stable measurements with noise levels of $42\,\mathrm{nm\,s^{-2}\,Hz^{-1/2}}$ and $0.5\,\mathrm{nm\,s^{-2}}$ after averaging, as demonstrated in atom interferometric gravimeters (Ménoret et al., 2018; Freier et al., 2016; Hu et al., 2013; Louchet-Chauvet et al., 2011; Peters et al., 1999). Operation in a microgravity environment could boost the sensitivity of such sensors by increasing the free-fall time of the atoms during the interferometry sequence, a critical parameter for the scaling factor (Kasevich and Chu, 1991), leading to anticipated noise levels of $0.1\,\mathrm{nm\,s^{-2}\,Hz^{-1/2}}$ and below (Dickerson et al., 2013). Multiple experiments implemented and investigated atom optics and atom interferometry in microgravity, including the production of Bose–Einstein condensates followed by a matter-wave collimation step, enabling the ultra-low expansion rates of the atomic ensembles for compatibility with extended free-fall times (Gaaloul et al., 2022; Lachmann et al., 2021; Aveline et al., 2020; Becker et al., 2018; Rudolph et al., 2015; Müntinga et al., 2013; Geiger et al., 2011; van Zoest et al., 2010). Operating atom interferometers at high data rates currently either implies an increased noise level due to short free-fall times (Rakholia et al., 2014) or an increased complexity when implementing an interleaved mode (Savoie et al., 2018). An alternative is the hybridization with an additional sensor to realize a combined drift-free system with sufficient bandwidth (Zahzam et al., 2022; Richardson et al., 2020; Lautier et al., 2014). The usage in inertial measurement units requires additional investigation, which is in synergy with current developments for an Earth-orbit gravity mission.

The AI system detection bandwidth is limited by the Nyquist sampling criterion to half the measurement repetition rate. In order to increase the bandwidth, a supplemental sensor will be used with the AI system. Optomechanical inertial sensors (OMIS) combine high precision displacement metrology with a low-noise mechanical oscillator to detect input acceleration down to the thermal noise limit with a bandwidth of several kHz or more. These sensors can be directly constructed into the AI retro-reflecting mirror to provide excellent overlap of their common reference frames easing correlation analysis between the two systems. Further, the optical source can be shared between the two systems, if desired, for reducing payload size. OMIS share a lot of features with optical cavity based frequency references such as low drift and high measurement precision. Additionally, the calibration parameters are tied to the stability of the onboard clock source and this is often the most precise and stable device in the system. This combination of features improves the low-frequency portion of the OMIS bandwidth enough to provide good overlap with demonstrated AI system bandwidths at a similar level of measurement imprecision. In this way, the AI can provide drift control of the OMIS while the OMIS provides high speed measurement of the residual accelerations affecting the satellite. Such hybrid systems have been proposed for different applications (Warner et al., 2019; Richardson et al., 2020)

Pointing: The accuracy of the measurement depends on the knowledge of the orbit (see below) and the alignment of the satellites to ground.

Several techniques exist to establish the necessary precision to achieve the scientific goals.

The alignment of the satellites can be regularly controlled by using the atom interferometer in regular intervals as a gradiometer. For this purpose, a secondary atom cloud needs to be suspended radially above the first. If the measured gravity gradient is not in line with predictions, the satellite alignment has to be corrected. While this method is certainly intriguing, classical means are foreseen for MaQuIs.

Propulsion: As part of the attitude and orbital control (AOCS), the amount of necessary propulsion as well as the positioning will have to be discussed. MaQuIs will fly in a low orbit and orbital corrections as well as alignment corrections will become necessary. For this purpose additional propulsion and appropriate thruster will be implemented. This part of the payload is mentioned here as it could prove an important mass driver.

Spacecraft Positioning: The orbit of satellites around other planetary bodies are usually determined by radio Doppler measurements from the Earth. The X-band Doppler radio accuracy for the Mars Reconnaissance Orbiter (MRO) is in the order of $0.05\,\text{mm}\,\text{s}^{-1}$ (Genova et al., 2016) depending on Sun-Earth-Mars angle. The requirement (3σ) for the MRO spacecrafts relative position to Mars is $100\,\text{m}$ in the along track, $40\,\text{m}$ cross track and $1.5\,\text{m}$ in the radial direction. Results from the mission show and RMS of $3.9\,\text{m}$, $0.6\,\text{m}$ and $0.9\,\text{m}$ respectively (Highsmith et al., 2008). For MaQuIs, we do not consider tracking-based gravity field solutions. For GRACE and GRACE-FO, GNSS data mainly help the estimation of the low degree coefficients of the gravity field model, which suffer from the bias and scale factor uncertainty of the capacitive accelerometers (Cheng and Ries, 2017). We do not expect this to be critical for MaQuIs given the cold atom inertial sensors and the use of the gravimetric data to study high-frequency features of Mars' gravity. Therefore, the position uncertainty does not translate directly into gravity field uncertainty (provided the orbit is sufficiently accurate for areo-location), it is expected that a typical two-way coherent X-band Doppler link will be sufficient, and accuracy enhancements from for instance X/Ka-band tracking as is done for BepiColombo (Iess et al., 2021) will not be necessary. Possible complementary range and VLBI data will not help to improve the spacecraft orbits w.r.t Mars, but would be beneficial for continued improvement of the Martian ephemeris (Dirkx et al., 2017, 2019), and possible orbit validation.

The orbit determination also depends on variation of center of mass (COM) with respect to the radio antenna phase centre (Cascioli and Genova, 2021), which can be in the decimeter range (Genova et al., 2016) e. g. due to orientation changes of the radio antenna to ensure its pointing towards the Earth or rotations of the solar panels to align with the Sun. For spacecraft like the MRO with a movable high gain antenna and solar panels (see Fig. 8), a mechanical model is required to calculate the COM depending on the mass distribution of the satellite components and its fuel consumption (Cascioli and Genova, 2021).

On a number of recent missions, such as BepiColombo and JUICE, an accelerometer is used to measure non-conservative forces, including variations of the change in spacecraft centre of mass due to for instance effects of propellant sloshing (Cascioli and Genova, 2021; Iess et al., 2021).

These aspects have not been an issue with terrestrial satellite gravimetry missions, because offsets between star cameras, GNSS antennas and the CMO are relatively static during one orbit due to fixed solar panels and antennas (see Fig. 5). However, for MaQuIs the aforementioned considerations might become relevant. The requirement for the GRACE-FO mission for the short term stability (one orbit) of the COM with respect to the accelerometer test mass is $\pm 9\,\mu\text{m}$. Long term variations (six months) of COM movements, e. g. due to fuel consumption, are kept within $\pm 100\,\mu\text{m}$ by employing movable mass trim mechanisms (Kornfeld et al., 2019). The evaluation of GRACE-FO LRI data has shown the ability of the attitude and orbit control system (AOCS) to maintain the pitch and yaw variations of the satellite
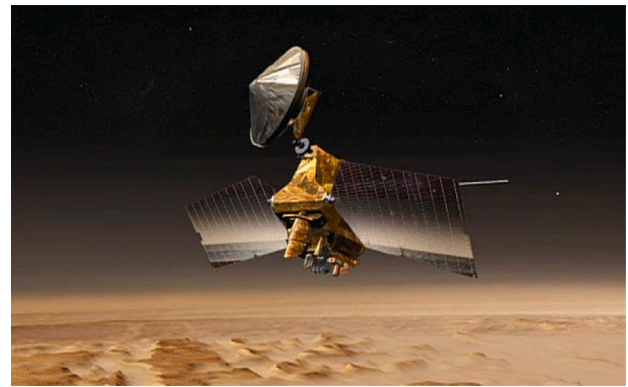

Fig. 8. Mars Reconnaissance Orbiter (artist rendering, credit NASA/JPL-Caltech) with a $3\,\text{m}$ High Gain Antenna and $10\,\text{m}^2$ solar panels.

pair within $\pm 100\,\mu\text{rad}$ (Goswami et al., 2021), which is the technical requirement of the LRI. Additionally, the combination of differential wavefront sensing and the beam steering mechanism with the star camera and IMU show the potential for an improved accuracy for attitude determination.

In conclusion, it is reasonable to assume that the achievable positioning accuracy is sufficient to allow the recovery of the searched gravitational field data. However, it is necessary to investigate positioning requirements and possibilities and their impact on the mission prior to designing the payload.

Mission Lifetime: One of the limitations of the mission is its lifetime. To measure the gravitational field distribution, an orbit, as close as possible to the surface is preferential. In the case of GRAIL, for instance, a low orbit over the lunar surface, with only $30\,\text{km}$ height was chosen (Zuber et al., 2013). This was possible due to the lack of atmosphere on the moon. In case of GRACE, GRACE-FO, and GOCE higher altitudes had to be chosen to allow for the required mission lifetimes within Earths atmosphere. Similar considerations have to be taken into account for MaQuIs.

Additionally, Mars poses the challenge of dust contamination of instrumentation. This posed a challenge especially for Rovers or other surface vehicles. With drag being one of the main issues, the final orbit will probably be high enough for dust to be a minor issue.

The final orbital considerations will be a trade-off between atmospheric drag, available fuel, acceptable vibrations, dust contamination, and required mission lifetime.

At this time a mission lifetime of at least two Martian years is planned. This allows for the study of annual processes and enable comparability between two sets of measurements in a given annual position. This choice has implications on a reasonable orbital altitude, satellite design, as well as fuel-consumption.

Power Consumption: As it has been discussed above, the mission life time is impacted by various different aspects. In addition to those, power consumption will become one of the major trade-off drivers. The increased distance to the Sun results in lower power levels. Usually, this could be battled by adding more solar panels, but the use of deployable structures should be minimized to reduce structural microvibrations, which corrupt the measurements collected by the cold atom inertial sensor. For MaQuIs, however, additional restraints based on atmospheric drag and the inability of using deployable structures (to minimize structural vibrations) have to be taken into account. Those have been discussed above and will have a major impact on payload allowances in terms of power consumption.

In combination with radiation hardness and miniaturization efforts, this leads to MaQuIs being an important pathfinder for the usage of quantum sensors in deep-space.

4.5.2. Additional instruments

Mass Spectrometer: The primary Instrument is the laser ranging facility including the supporting technology. In addition, knowledge of the atmospheric density and composition at the orbit is important. It is therefore conceivable to include a mass spectrometer in the payload.

The atmospheric disturbances could also be measured using the atom interferometer without the additional mass spectrometer. The drag on the satellites yields information on atmospheric density and phenomena such as gravity waves (Starichenko et al., 2021) within those. Consequently, measuring the forces acting on the satellite allows scientific studies of the Martian atmosphere and its dynamics in addition to the gravitational field mapping.

Imaging Technology: As it is mentioned above, the gravitational data should be supplemented with imaging data. The correlation between images and the recorded gravitational data yields the information on the ground below. Of course, several high-resolution images of Mars exist. To supplement the gravitational data and account for any temporal changes, an additional camera on MaQuIs is beneficial. As, in addition, available cameras are not taking up a high portion of the available size, mass, and power budget. Consequently, flying a camera on MaQuIs will allow to correlate the gravity data directly to images taken during flight. Space qualified cameras are readily available and should be implemented into the payload. However, constraints on mass, size, or power could prove too restrictive to include a camera. At this moment, a camera is foreseen for flight. It might later be removed from the payload.

4.5.3. Technology readiness level

Currently, the items in the payload are advanced with respect to the technology readiness level (TRL) and promise reliable operation and precise measurements. The least evolved system is the atom interferometer, allowing for the drift-free correction of the inertial measurement unit. As it is described above, condensed atom ensembles have already been deployed in space. The adaptations necessary to deploy such a system in space are supported and with similar missions planned for Earth, the technology will be readily available at the time of launch for MaQuIs. For example, the European Commission's stated goal is to launch a pathfinder mission to demonstrate a working quantum accelerometer in space by 2030. A consortium organized by the French and German space agencies is currently working on the CARIOQA – Pathfinder Mission Preparation project, funded under the Horizon Europe programme. The project aims to develop an engineering model of a quantum accelerometer and is investigating Earth observation user needs and potential quantum space gravimetry mission scenarios to meet these needs. A Horizon Europe-funded Phase A study for the quantum pathfinder mission, also called CARIOQA (Lévèque et al., 2022), will be carried out in 2024. This study will identify the steps necessary to raise the TRL of the required technologies to TRL 5. The aim of the European commission is to launch a pathfinder mission, based on the CARIOQA developments, in the early 2030s (CARIOQA Project Website).

For most of the other components, commercial, space qualified items are available or other hardware with space heritage exists. While MaQuIs will opt for non-qualified items, for all items a qualified option exists, that could be exchanged if the technology proves too immature. This is especially true, since the system will fly in a GRACE-configuration and could therefore rely on the developments for GRACE, GRACE-FO, and GRAIL.

Additional developments of the required technologies are outlined in the cold atoms road map (Alonso et al., 2022). This shows the increased interest in cold atom technology for scientific and applied missions and the required developments to establish the necessary systems for different missions. MaQuIs both, benefits from and drives these developments.

4.6. Noise sources

The missions success relies on understanding noise sources and mitigating their impact. The discussed noise sources in this proposal are:

- Residual accelerations of the satellites leads to an incorrect measurement. To correct for this, two inertial measurement units are proposed for MaQuIs. An additional means of reducing the impact of atmospheric drag is the satellite design, similar to the GOCE mission (Rummel et al., 2011)
- Undetected orbital variations will lead to a difference in the measured signal and thereby in a faulty analysis of the data in post processing. Orbital surveillance and correction are therefore paramount for the success of the mission.
- The laser wavelength deployed for the link between the two satellites determines the accuracy of the measurement. Hence, knowledge about its absolute value in orbit is required.
- Due to the unequal arm lengths of the laser interferometer that shall be used for the inter-satellite distance measurements, laser frequency noise dominates the range measurement. Bachman et al. (2017), Müller et al. (2022) MaQuIs will deploy optical frequency references to increase the laser stability.
- Thermal fluctuations impact several systems of the satellites resulting in an elevated noise floor.
- Cosmic radiation and light pollution can lead to damage in the system or faulty measurements.

5. Additional gradiometer

On Earth, the only satellite gradiometry mission flown to date was GOCE (Rummel et al., 2011), which determined the global static gravity field with unprecedented accuracy. The noise of the gradiometer axes was approximately $10 \, \mathrm{mE}/\sqrt{\mathrm{Hz}}$. Further improvements or resolving temporal variations of the gravity field would require major improvements in the satellite design and a reduction of the measurement noise to $5 \, \mathrm{mE}/\sqrt{\mathrm{Hz}}$ or below. In parallel to studies investigating cold atom interferometry on GRACE-FO type missions, in which the cold atom interferometer acts as a accelerometer, gradiometry mission designs based on quantum technologies are also the topic of numerous studies. A quantum gradiometer employs two spatially separated clouds of (ultra-)cold atoms which interact with the same laser beams. This requires a vacuum chamber of a size to accommodate the desired separation, e. g. 50 cm for each axis.

The works by, for example, Douch et al. (2018),Trimeche et al. (2019) and Migliaccio et al. (2019, 2022) discuss different scenarios for employing GOCE type mission scenarios utilizing a cold atom interferometer based single axis gradiometer. The proposed instrument and mission designs show a clear benefit in determining temporal gravity field variations as well as geophysical processes when compared to GOCE and in some scenarios even GRACE. However, the main technical challenges, in addition to realizing a gradiometer in space, arise from the rotation of the satellite about its along track axis (Lan et al., 2012). A full 3-axis gradiometer could solve this challenge while increasing the complexity of the instrument. A discussion on the rotation of an along track quantum accelerometer can be found, e. g., in Meister et al. (2022). A compromise in the gradiometer design would be a single axis gradiometer in the cross track direction, greatly reducing rotational effects but not sufficient on its own to exceed GOCE performance levels (Douch et al., 2018), employed on GRACE like mission (Rosen, 2021). This design adds observations perpendicular to the LRI measurements thereby effectively reducing the aliasing errors in GRACE solutions commonly referred to as striping effect.

6. Summary and outlook

The Mars Quantum Gravity Mission (MaQuIs) targets Mars and its gravitational field to investigate the planet for subsurface water occurrences. With this capability, MaQuIs is qualified to contribute to the discussion around the occurrence of liquid or frozen subsurface water on Mars. Furthermore, the study of the gravitational field yields information on planetary dynamics and seasonal changes, interesting for planetary research.

In this paper, we discussed the current knowledge of the Martian gravity field and identified research questions, which can be addressed by a dedicated satellite gravimetry mission. We presented the currently available technologies to execute such a complex gravitational field measurement to improve the available gravitational maps using quantum technologies.

Similar to Earth-observation, the gravitational field of Mars could also be mapped using a gravity gradiometer. This lowers the design complexity on two-satellite alignment and reduces the power and size requirements set by the payload. MaQuIs however, focuses on inter-satellite ranging gravimetry with a Mars gravity gradiometer being a possible alternative route to be studied in the future. We have chosen this course because, for time variable gravimetry on Earth, the sensitivity requirements for the accelerometers used in gradiometry are 2 to 3 orders of magnitude larger than for inter-satellite ranging, and we expect this to be the same for Mars. The next step for this mission concept is the simulation of scenarios applying the technologies discussed in this paper and evaluate the impact on gravity field products. Dependencies between different mission parameters, for example, orbit height and expected gravity signal on the one hand and satellite geometry, atmospheric drag and mission lifetime on the other will be investigated. Limiting factors for the concept and technologies based in the Martian environment will be identified and mitigation strategies and trade offs be considered. The mission scenarios will be evaluated for their scientific gain with regards to, amongst others, the scientific goals defined herein as a basis for future steps.

CRediT authorship contribution statement

L. Wörner: Assembled the consortium. **B.C. Root:** Estimated the expected gravitational signal, Discussed the scientific gain of a gravitational measurement of Mars, Described the required resolution and added vital information on Mars, Calculated the error estimates. **P. Bouyer:** Added the details on the inertial measurement system proposed for the mission. **C. Braxmaier:** Added the details on the inertial measurement system proposed for the mission. **D. Dirkx:** Estimated the expected gravitational signal, Calculated the error estimates. **J. Encarnação:** Estimated the expected gravitational signal, Discussed the scientific gain of a gravitational measurement of Mars, Described the required resolution and added vital information on Mars, Calculated the error estimates. **E. Hauber:** Discussed the scientific gain of a gravitational measurement of Mars, Described the required resolution and added vital information on Mars. **H. Hussmann:** Discussed the scientific gain of a gravitational measurement of Mars, Described the required resolution and added vital information on Mars, Calculated the error estimates. **Ö. Karatekin:** Discussed the scientific gain of a gravitational measurement of Mars, Described the required resolution and added vital information on Mars. **A. Koch:** Inserted the primary measurement method, Calculated the error estimates. **L. Kumanchik:** Added the details on the inertial measurement system proposed for the mission. **F. Migliaccio:** Estimated the expected gravitational signal. **M. Reguzzoni:** Estimated the expected gravitational signal. **B. Ritter:** Discussed the scientific gain of a gravitational measurement of Mars, Described the required resolution and added vital information on Mars. **M. Schilling:** Estimated the expected gravitational signal, Calculated the error estimates. **C. Schubert:** Added the details on the inertial measurement system proposed for the mission. **C. Thieulot:** Discussed

the scientific gain of a gravitational measurement of Mars, Described the required resolution and added vital information on Mars. **W.v. Klitzing:** Added the details on the inertial measurement system proposed for the mission. **O. Witasse:** Discussed the scientific gain of a gravitational measurement of Mars, Described the required resolution and added vital information on Mars, Assembled the consortium.

Declaration of competing interest

The authors declare that they have no known competing financial interests or personal relationships that could have appeared to influence the work reported in this paper.

Data availability

No data was used for the research described in the article.

References

Abich, K., Abramovici, A., Amparan, B., Baatzsch, A., Okihiro, B.B., Barr, D.C., Bize, M.P., Bogan, C., Braxmaier, C., et al., 2019. In-orbit performance of the GRACE follow-on laser ranging interferometer. Phys. Rev. Lett. 123 (3), 031101. http://dx.doi.org/10.1103/PhysRevLett.123.031101.

Alonso, I., Alpigiani, C., Altschul, B., Araújo, H., Arduini, G., Arlt, J., Badurina, L., Balaž, A., Bandarupally, S., Barish, B.C., Barone, M., Barsanti, M., Bass, S., Bassi, A., Battelier, B., Baynham, C.F.A., Beaufils, Q., Belić, A., Bergé, J., Bernabeu, J., Bertoldi, A., Bingham, R., Bize, S., Blas, D., Bongs, K., Bouyer, P., Braitenberg, C., Brand, C., Braxmaier, C., Bresson, A., Buchmueller, O., Budker, D., Bugalho, L., Burdin, S., Cacciapuoti, L., Callegari, S., Calmet, X., Calonico, D., Canuel, B., Caramete, L.-I., Carraz, O., Cassettari, D., Chakraborty, P., Chattopadhyay, S., Chauhan, U., Chen, X., Chen, Y.-A., Chiofalo, M.L., Coleman, J., Corgier, R., Cotter, J.P., Michael Cruise, A., Cui, Y., Davies, G., De Roeck, A., Demarteau, M., Derevianko, A., Di Clemente, M., Djordjevic, G.S., Donadi, S., Doré, O., Dornan, P., Doser, M., Drougakis, G., Dunningham, J., Easo, S., Eby, J., Elertas, G., Ellis, J., Evans, D., Examilioti, P., Fadeev, P., Fanì, M., Fassi, F., Fattori, M., Fedderke, M.A., Felea, D., Feng, C.-H., Ferreras, J., Flack, R., Flambaum, V.V., Forsberg, R., Fromhold, M., Gaaloul, N., Garraway, B.M., Georgousi, M., Geraci, A., Gibble, K., Gibson, V., Gill, P., Giudice, G.F., Goldwin, J., Gould, O., Grachov, O., Graham, P.W., Grasso, D., Griffin, P.F., Guerlin, C., Gündoğan, M., Gupta, R.K., Haehnelt, M., Hanımeli, E.T., Hawkins, L., Hees, A., Henderson, V.A., Herr, W., Herrmann, S., Hird, T., Hobson, R., Hock, V., Hogan, J.M., Holst, B., Holynski, M., Israelsson, U., Jeglič, P., Jetzer, P., Juzeliūnas, G., Kaltenbaek, R., Kamenik, J.F., Kehagias, A., Kirova, T., Kiss-Toth, M., Koke, S., Kolkowitz, S., Kornakov, G., Kovachy, T., Krutzik, M., Kumar, M., Kumar, P., Lämmerzahl, C., Landsberg, G., Le Poncin-Lafitte, C., Leibrandt, D.R., Lévèque, T., Lewicki, M., Li, R., Lipniacka, A., Lisdat, C., Liu, M., Lopez-Gonzalez, J.L., Loriani, S., Louko, J., Luciano, G.G., Lundblad, N., Maddox, S., Mahmoud, M.A., Maleknejad, A., March-Russell, J., Massonnet, D., McCabe, C., Meister, M., Mežnaršič, T., Micalizio, S., Migliaccio, F., Millington, P., Milosevic, M., Mitchell, J., Morley, G.W., Müller, J., Murphy, E., Müstecaplıoğlu, Ö.E., O'Shea, V., Oi, D.K.L., Olson, J., Pal, D., Papazoglou, D.G., Pasatembou, E., Paternostro, M., Pawlowski, K., Pelucchi, E., Pereira dos Santos, F., Peters, A., Pikovski, I., Pilaftsis, A., Pinto, A., Prevedelli, M., Puthiya-Veettil, V., Quenby, J., Rafelski, J., Rasel, E.M., Ravensbergen, C., Reguzzoni, M., Richaud, A., Riou, I., Rothacher, M., Roura, A., Ruschhaupt, A., Sabulsky, D.O., Safronova, M., Saltas, I.D., Salvi, L., Sameed, M., Saurabh, P., Schäffer, S., Schiller, S., Schilling, M., Schkolnik, V., Schlippert, D., Schmidt, P.O., Schnatz, H., Schneider, J., Schneider, U., Schreck, F., Schubert, C., Shayeghi, A., Sherrill, N., Shipsey, I., Signorini, C., Singh, R., Singh, Y., Skordis, C., Smerzi, A., Sopuerta, C.F., Sorrentino, F., Sphicas, P., Stadnik, Y.V., Stefanescu, P., Tarallo, M.G., Tentindo, S., Tino, G.M., Tinsley, J.N., Tornatore, V., Treutlein, P., Trombettoni, A., Tsai, Y.-D., Tuckey, P., Uchida, M.A., Valenzuela, T., Van Den Bossche, M., Vaskonen, V., Verma, G., Vetrano, F., Vogt, C., von Klitzing, W., Waller, P., Walser, R., Wille, E., Williams, J., Windpassinger, P., Wittrock, U., Wolf, P., Woltmann, M., Wörner, L., Xuereb, A., Yahia, M., Yazgan, E., Yu, N., Zahzam, N., Zambrini Cruzeiro, E., Zhan, M., Zou, X., Zupan, J., Zupanič, E., 2022. Cold atoms in space: community workshop summary and proposed road-map. EPJ Quantum Technol. 9 (1), 30. http://dx.doi.org/10.1140/epjqt/s40507-022-00147-w.

Antonucci, F., Armano, M., Audley, H., Auger, G., Benedetti, M., Binetruy, P., Bogenstahl, J., Bortoluzzi, D., Bosetti, P., Brandt, N., et al., 2012. The LISA Pathfinder mission. Classical Quantum Gravity 29 (12), 124014. http://dx.doi.org/10.1088/0264-9381/29/12/124014.

Aveline, D.C., Williams, J.R., Elliott, E.R., Dutenhoffer, C., Kellogg, J.R., Kohel, J.M., Lay, N.E., Oudrhiri, K., Shotwell, R.F., Yu, N., Thompson, R.J., 2020. Observation of Bose-Einstein condensates in an Earth-orbiting research lab. Nature 582 (7811), 193–197. http://dx.doi.org/10.1038/s41586-020-2346-1.

Bachman, B., de Vine, G., Dickson, J., Dubovitsky, S., Liu, J., Klipstein, W., McKenzie, K., Spero, R., Sutton, A., Ware, B., Woodruff, C., 2017. Flight phasemeter on the Laser Ranging Interferometer on the GRACE Follow-On mission. IOP Conf. Ser. J. Phys. Conf. Ser. 840, 012011. http://dx.doi.org/10.1088/1742-6596/840/1/012011.

Banerdt, W.B., Smrekar, S.E., Banfield, D., Giardini, D., Golombek, M., Johnson, C.L., Lognonné, P., Spiga, A., Spohn, T., Perrin, C., et al., 2020. Initial results from the InSight mission on Mars. Nat. Geosci. 13 (3), 183–189. http://dx.doi.org/10.1038/s41561-020-0544-y.

Becker, D., Lachmann, M.D., Seidel, S.T., Ahlers, H., Dinkelaker, A.N., Grosse, J., Hellmig, O., Müntinga, H., Schkolnik, V., Wendrich, T., Wenzlawski, A., Weps, B., Corgier, R., Franz, T., Gaaloul, N., Herr, W., Lüdtke, D., Popp, M., Amri, S., Duncker, H., Erbe, M., Kohfeldt, A., Kubelka-Lange, A., Braxmaier, C., Charron, E., Ertmer, W., Krutzik, M., Lämmerzahl, C., Peters, A., Schleich, W.P., Sengstock, K., Walser, R., Wicht, A., Windpassinger, P., Rasel, E.M., 2018. Space-borne bose–Einstein condensation for precision interferometry. Nature 562, 391–395. http://dx.doi.org/10.1038/s41586-018-0605-1.

Belenchia, A., Carlesso, M., Bayraktar, Ö., Dequal, D., Derkach, I., Gasbarri, G., Herr, W., Li, Y.L., Rademacher, M., Sidhu, J., Oi, D.K., Seidel, S.T., Kaltenbaek, R., Marquardt, C., Ulbricht, H., Usenko, V.C., Wörner, L., Xuereb, A., Paternostro, M., Bassi, A., 2022. Quantum physics in space. Phys. Rep. 951, 1–70. http://dx.doi.org/10.1016/j.physrep.2021.11.004.

Belleguic, V., Lognonné, P., Wieczorek, M., 2005. Constraints on the Martian lithosphere from gravity and topography data. J. Geophys. Res. Planets 110, E11005. http://dx.doi.org/10.1029/2005JE002437.

Beuthe, M., Le Maistre, S., Rosenblatt, P., Pätzold, M., Dehant, V., 2012. Density and lithospheric thickness of the Tharsis Province from MEX MaRS and MRO gravity data. J. Geophys. Res. Planets 117, E04002. http://dx.doi.org/10.1029/2011JE003976.

Bibring, J.-P., Langevin, Y., Mustard, J.F., Poulet, F., Arvidson, R., Gendrin, A., Gondet, B., Mangold, N., Pinet, P., Forget, F., Berthé, M., Bibring, J.-P., Gendrin, A., Gomez, C., Gondet, B., Jouglet, D., Poulet, F., Soufflot, A., Vincendon, M., Combes, M., Drossart, P., Encrenaz, T., Fouchet, T., Merchiorri, R., Belluci, G., Altieri, F., Formisano, V., Capaccioni, F., Cerroni, P., Coradini, A., Fonti, S., Korablev, O., Kottsov, V., Ignatiev, N., Moroz, V., Titov, D., Zasova, L., Loiseau, D., Mangold, N., Pinet, P., Douté, S., Schmitt, B., Sotin, C., Hauber, E., Hoffmann, H., Jaumann, R., Keller, U., Arvidson, R., Mustard, J.F., Duxbury, T., Forget, F., Neukum, G., 2006. Global mineralogical and aqueous Mars history derived from OMEGA/Mars Express data. Science 312 (5772), 400–404. http://dx.doi.org/10.1126/science.1122659.

Bierson, C.J., Tulaczyk, S., Courville, S.W., Putzig, N.E., 2021. Strong MARSIS radar reflections from the base of Martian south polar cap may be due to conductive ice or minerals. Geophys. Res. Lett. 48 (13), e93880. http://dx.doi.org/10.1029/2021GL093880.

Bills, B.G., Ermakov, A.I., 2019. Simple models of error spectra for planetary gravitational potentials as obtained from a variety of measurement configurations. Planet. Space Sci. 179, 104744. http://dx.doi.org/10.1016/j.pss.2019.104744, URL https://www.sciencedirect.com/science/article/pii/S003206331830432X.

Bott, M.H.P., 1960. The use of rapid digital computing methods for direct gravity interpretation of sedimentary basins. Geophys. J. 3 (1), 63–67. http://dx.doi.org/10.1111/j.1365-246X.1960.tb00065.x.

Bouley, S., Baratoux, D., Matsuyama, I., Forget, F., Séjourné, A., Turbet, M., Costard, F., 2016. Late Tharsis formation and implications for early Mars. Nature 531 (7594), 344–347. http://dx.doi.org/10.1038/nature17171.

Bouman, J., Ebbing, J., Fuchs, M., 2013. Reference frame transformation of satellite gravity gradients and topographic mass reduction. J. Geophys. Res. Solid Earth 118 (2), 759–774. http://dx.doi.org/10.1029/2012JB009747.

Breuer, D., Spohn, T., van Hoolst, T., van Westrenen, W., Stanley, S., Rambaux, N., 2022. Interiors of Earth-like planets and satellites of the solar system. Surv. Geophys. 43 (1), 177–226. http://dx.doi.org/10.1007/s10712-021-09677-x.

Broquet, A., Andrews-Hanna, J.C., 2022. Geophysical evidence for an active mantle plume underneath Elysium Planitia on Mars. Nat. Astron. http://dx.doi.org/10.1038/s41550-022-01836-3.

Brož, P., Hauber, E., van de Burgt, I., Å pillar, V., Michael, G., 2019. Subsurface sediment mobilization in the southern Chryse Planitia on Mars. J. Geophys. Res. (Planets) 124 (3), 703–720. http://dx.doi.org/10.1029/2018JE005868.

Byrne, S., 2009. The polar deposits of Mars. Ann. Rev. Earth Planet. Sci. 37 (1), 535–560. http://dx.doi.org/10.1146/annurev.earth.031208.100101.

Cappuccio, P., Di Ruscio, A., Iess, L., Mariani, M.J., 2020. BepiColombo gravity and rotation experiment in a Pseudo drag-free system. In: AIAA Scitech 2020 Forum. American Institute of Aeronautics and Astronautics, http://dx.doi.org/10.2514/6.2020-1095.

CARIOQA Project Website, 2023. URL https://carioqa-quantumpathfinder.eu/quantum-pathfinder-mission/.

Carr, M.H., Head, J.W., 2015. Martian surface/near-surface water inventory: Sources, sinks, and changes with time. Geophys. Res. Lett. 42 (3), 726–732. http://dx.doi.org/10.1002/2014GL062464.

Carraz, O., Siemes, C., Massotti, L., Haagmans, R., Silvestrin, P., 2014. A spaceborne gravity gradiometer concept based on cold atom interferometers for measuring Earth's gravity field. Microgravity Sci. Technol. 26 (3), 139–145. http://dx.doi.org/10.1007/s12217-014-9385-x.

Carter, J., Riu, L., Poulet, F., Bibring, J.-P., Langevin, Y., Gondet, B., 2023. A mars orbital catalog of aqueous alteration signatures (MOCAAS). Icarus 389, 115164. http://dx.doi.org/10.1016/j.icarus.2022.115164.

Cascioli, G., Genova, A., 2021. Precise orbit determination technique to refine spacecraft mechanical modeling. J. Spacecr. Rockets 58 (2), 581–588. http://dx.doi.org/10.2514/1.A34922.

Castellini, F., Bellei, G., Godard, B., 2018. Flight dynamics operational experience from Exomars TGO aerobraking campaign at Mars. In: 2018 SpaceOps Conference. 28.05.-01.06.2018, Marseille, France, American Institute of Aeronautics and Astronautics, http://dx.doi.org/10.2514/6.2018-2537.

Cheng, M., Ries, J., 2017. The unexpected signal in GRACE estimates of C20. J. Geod. 91 (8), 897–914. http://dx.doi.org/10.1007/s00190-016-0995-5.

Chiow, S.W., Williams, J., Yu, N., 2015. Laser-ranging long-baseline differential atom interferometers for space. Phys. Rev. A 92 (6), 063613. http://dx.doi.org/10.1103/PhysRevA.92.063613.

Christophe, B., Boulanger, D., Foulon, B., Huynh, P.A., Lebat, V., Liorzou, F., Perrot, E., 2015. A new generation of ultra-sensitive electrostatic accelerometers for GRACE Follow-on and towards the next generation gravity missions. Acta Astronaut. 117, 1–7. http://dx.doi.org/10.1016/j.actaastro.2015.06.021.

Clifford, S.M., Lasue, J., Heggy, E., Boisson, J., McGovern, P., Max, M.D., 2010. Depth of the martian cryosphere: Revised estimates and implications for the existence and detection of subpermafrost groundwater. J. Geophys. Res. (Planets) 115 (E7), E07001. http://dx.doi.org/10.1029/2009JE003462.

Cuřín, V., Brož, P., Hauber, E., Markonis, Y., 2023. Mud flows in southwestern Utopia Planitia, Mars. Icarus 389, 115266. http://dx.doi.org/10.1016/j.icarus.2022.115266.

Dahl, C., Baatzsch, A., Dehne, M., Herding, M., Nicklaus, K., Braxmaier, C., Sanjuan, J., Zender, B., Barranco, G.F., Schütze, D., Stede, G., Gilles, F., Hager, P., Voss, K., Abich, K., Gohlke, M., Guenther, B., Görth, A., Mahrdt, C., Müller, V., Heinzel, G., 2016. Laser ranging interferometer on Grace Follow-On. In: Cugny, B., Karafolas, N., Sodnik, Z. (Eds.), International Conference on Space Optics. ICSO 2016, 18.-21.10.2016, Biarritz, France, In: Proc. of SPIE, vol. 10562, http://dx.doi.org/10.1117/12.2297705.

Dickerson, S.M., Hogan, J.M., Sugarbaker, A., Johnson, D.M.S., Kasevich, M.A., 2013. Multiaxis inertial sensing with long-time point source atom interferometry. Phys. Rev. Lett. 111 (8), 083001. http://dx.doi.org/10.1103/PhysRevLett.111.083001.

Dirkx, D., Gurvits, L.I., Lainey, V., Lari, G., Milani, A., Cimò, G., Bocanegra-Bahamon, T., Visser, P., 2017. On the contribution of PRIDE-JUICE to Jovian system ephemerides. Planet. Space Sci. 147, 14–27. http://dx.doi.org/10.1016/j.pss.2017.09.004.

Dirkx, D., Prochazka, I., Bauer, S., Visser, P., Noomen, R., Gurvits, L.I., Vermeersen, B., 2019. Laser and radio tracking for planetary science missions—a comparison. J. Geod. 93 (11), 2405–2420. http://dx.doi.org/10.1007/s00190-018-1171-x.

Dirkx, D., Vermeersen, L., Noomen, R., Visser, P., 2014. Phobos laser ranging: numerical geodesy experiments for Martian system science. Planet. Space Sci. 99, 84–102. http://dx.doi.org/10.1016/j.pss.2014.03.022.

Doo, W.-B., Hsu, S.-K., Lo, C.-L., Chen, S.-C., Tsai, C.-H., Lin, J.-Y., Huang, Y.-P., Huang, Y.-S., Chiu, S.-D., Ma, Y.-F., 2015. Gravity anomalies of the active mud diapirs off southwest Taiwan. Geophys. J. Int. 203 (3), 2089–2098. http://dx.doi.org/10.1093/gji/ggv430.

Doornbos, E., 2012. Thermospheric Density and Wind Determination from Satellite Dynamics (Ph.D. thesis). Delft University of Technology, http://dx.doi.org/10.1007/978-3-642-25129-0.

Döringshoff, K., Schuldt, T., Kovalchuk, E.V., Stühler, J., Braxmaier, C., Peters, A., 2017. A flight-like absolute optical frequency reference based on iodine for laser systems at 1064 nm. Appl. Phys. B 123 (6), 183. http://dx.doi.org/10.1007/s00340-017-6756-1.

Douch, K., Wu, H., Schubert, C., Müller, J., Pereira dos Santos, F., 2018. Simulation-based evaluation of a cold atom interferometry gradiometer concept for gravity field recovery. Adv. Space Res. 61 (5), 1307–1323. http://dx.doi.org/10.1016/j.asr.2017.12.005.

Dundas, C.M., Mellon, M.T., Conway, S.J., Daubar, I.J., Williams, K.E., Ojha, L., Wray, J.J., Bramson, A.M., Byrne, S., McEwen, A.S., Posiolova, L.V., Speth, G., Viola, D., Landis, M.E., Morgan, G.A., Pathare, A.V., 2021. Widespread exposures of extensive clean shallow ice in the midlatitudes of Mars. J. Geophys. Res. (Planets) 126 (3), e06617. http://dx.doi.org/10.1029/2020JE006617.

Efroimsky, M., Lainey, V., 2007. Physics of bodily tides in terrestrial planets and the appropriate scales of dynamical evolution. J. Geophys. Res. Planets 112, E12003. http://dx.doi.org/10.1029/2007JE002908.

Fernández Barranco, G., Sheard, B.S., Dahl, C., Mathis, W., Heinzel, G., 2018. A low-power, low-noise 37-MHz photoreceiver for intersatellite laser interferometers using discrete heterojunction bipolar transistors. IEEE Sens. J. 18 (18), http://dx.doi.org/10.1109/JSEN.2018.2857202.

Folkner, W.M., Dehant, V., Le Maistre, S., Yseboodt, M., Rivoldini, A., Van Hoolst, T., Asmar, S.W., Golombek, M.P., 2018. The rotation and interior structure experiment on the InSight mission to Mars. Space Sci. Rev. 214 (5), 100. http://dx.doi.org/10.1007/s11214-018-0530-1.

Freier, C., Hauth, M., Schkolnik, V., Leykauf, B., Schilling, M., Wziontek, H., Scherneck, H.-G., Müller, J., Peters, A., 2016. Mobile quantum gravity sensor with unprecedented stability. J. Phys. Conf. Ser. 723, 012050. http://dx.doi.org/10.1088/1742-6596/723/1/012050.

Frey, H.V., Roark, J.H., Shockey, K.M., Frey, E.L., Sakimoto, S.E.H., 2002. Ancient lowlands on Mars. Geophys. Res. Lett. 29 (10), 1384. http://dx.doi.org/10.1029/2001GL013832.

Fryer, P., Wheat, C.G., Williams, T., Kelley, C., Johnson, K., Ryan, J., Kurz, W., Shervais, J., Albers, E., Bekins, B., Debret, B., Deng, J., Dong, Y., Eickenbusch, P., Frery, E., Ichiyama, Y., Johnston, R., Kevorkian, R., Magalhaes, V., Mantovanelli, S., Menapace, W., Menzies, C., Michibayashi, K., Moyer, C., Mullane, K., Park, J.-W., Price, R., Sissmann, O., Suzuki, S., Takai, K., Walter, B., Zhang, R., Amon, D., Glickson, D., Pomponi, S., 2020. Mariana serpentinite mud volcanism exhumes subducted seamount materials: implications for the origin of life. Philos. Trans. R. Soc. Lond. Ser. A 378 (2165), 20180425. http://dx.doi.org/10.1098/rsta.2018.0425.

Gaaloul, N., Meister, M., Corgier, R., Pichery, A., Boegel, P., Herr, W., Ahlers, H., Charron, E., Williams, J.R., Thompson, R.J., Schleich, W.P., Rasel, E.M., Bigelow, N.P., 2022. A space-based quantum gas laboratory at picokelvin energy scales. Nature Commun. 13, 7889. http://dx.doi.org/10.1038/s41467-022-35274-6.

Geiger, R., Ménoret, V., Stern, G., Zahzam, N., Cheinet, P., Battelier, B., Villing, A., Moron, F., Lours, M., Bidel, Y., et al., 2011. Detecting inertial effects with airborne matter-wave interferometry. Nature commun. 2, 474. http://dx.doi.org/10.1038/ncomms1479.

Genova, A., 2020. ORACLE: A mission concept to study Mars' climate, surface and interior. Acta Astronaut. 166, 317–329. http://dx.doi.org/10.1016/j.actaastro.2019.10.006.

Genova, A., Goossens, S., Lemoine, F.G., Mazarico, E., Neumann, G.A., Smith, D.E., Zuber, M.T., 2016. Seasonal and static gravity field of Mars from MGS, Mars Odyssey and MRO radio science. Icarus 272, 228–245. http://dx.doi.org/10.1016/j.icarus.2016.02.050.

Glassmeier, K.-H., 2020. Solar system exploration via comparative planetology. Nature Commun. 11 (1), 474. http://dx.doi.org/10.1038/s41467-020-18126-z.

Goossens, S., Sabaka, T.J., Genova, A., Mazarico, E., Nicholas, J.B., Neumann, G.A., 2017. Evidence for a low bulk crustal density for Mars from gravity and topography. Geophys. Res. Lett. 44 (15), 7686–7694. http://dx.doi.org/10.1002/2017GL074172.

Goossens, S., Sabaka, T.J., Wieczorek, M.A., Neumann, G.A., Mazarico, E., Lemoine, F.G., Nicholas, J.B., Smith, D.E., Zuber, M.T., 2020. High–resolution gravity field models from GRAIL data and implications for models of the density structure of the Moon's crust. J. Geophys. Res. Planets 125 (2), http://dx.doi.org/10.1029/2019JE006086.

Goswami, S., Francis, S.P., Bandikova, T., Spero, R.E., 2021. Analysis of GRACE Follow-On Laser Ranging Interferometer derived inter-satellite pointing angles. IEEE Sens. J. 21 (17), 19209–19221. http://dx.doi.org/10.1109/JSEN.2021.3090790.

Grimm, R.E., Harrison, K.P., Stillman, D.E., Kirchoff, M.R., 2017. On the secular retention of ground water and ice on Mars. J. Geophys. Res. (Planets) 122 (1), 94–109. http://dx.doi.org/10.1002/2016JE005132.

Haagmans, R., Siemes, C., Massotti, L., Carraz, O., Silvestrin, P., 2020. ESA's next-generation gravity mission concepts. Rend Lincei-Sci. Fis. 31, 15–25. http://dx.doi.org/10.1007/s12210-020-00875-0.

Haberle, M.R., Kahre, M.A., 2010. Detecting secular climate change on Mars. Int. J. Mars Sci. Explor. 5, 68–75. http://dx.doi.org/10.1555/mars.2010.0003.

Heggy, E., Paillou, P., Ruffie, G., Malezieux, J., Costard, F., Grandjean, G., 2001. On water detection in the Martian subsurface using sounding radar. Icarus 154 (2), 244–257. http://dx.doi.org/10.1006/icar.2001.6717.

Heinzel, G., Esteban, J.J., Barke, S., Markus, O., Wang, Y., Garcia, A.F., Danzmann, K., 2011. Auxiliary functions of the LISA laser link: ranging, clock noise transfer and data communication. Classical Quantum Gravity 28 (9), 094008. http://dx.doi.org/10.1088/0264-9381/28/9/094008.

Highsmith, D., You, T.-H., Demcak, S., Graat, E., Higa, E., Long, S., Bhat, R., Mottinger, N., Halsell, A., Peralta, F., 2008. Mars Reconnaissance Orbiter navigation during the primary science phase. In: AIAA/AAS Astrodynamics Specialist Conference. 18.-21.08.2008, Honolulu, Hawaii, USA, 092407. http://dx.doi.org/10.2514/6.2008-6422.

Holt, J.W., Safaeinili, A., Plaut, J.J., Head, J.W., Phillips, R.J., Seu, R., Kempf, S.D., Choudhary, P., Young, D.A., Putzig, N.E., Biccari, D., Gim, Y., 2008. Radar sounding evidence for buried glaciers in the southern mid-latitudes of Mars. Science 322 (5905), 1235. http://dx.doi.org/10.1126/science.1164246.

Hu, Z.-K., Sun, B.-L., Duan, X.-C., Zhou, M.-K., Chen, L.-L., Zhan, S., Zhang, Q.-Z., Luo, J., 2013. Demonstration of an ultrahigh-sensitivity atom-interferometry absolute gravimeter. Phys. Rev. A 88, 043610. http://dx.doi.org/10.1103/PhysRevA.88.043610.

Iess, L., Asmar, S.W., Cappuccio, P., Cascioli, G., de Marchi, F., Di Stefano, I., Genova, A., Ashby, N., Barriot, J.P., Bender, P., Benedetto, C., Border, J.S., Budnik, F., Ciarcia, S., Damour, T., Dehant, V., Di Achille, G., Di Ruscio, A., Fienga, A., Formaro, R., Klioner, S., Konopliv, A., Lemaître, A., Longo, F., Mercolino, M., Mitri, G., Notaro, V., Olivieri, A., Paik, M., Palli, A., Schettino, G., Serra, D., Simone, L., Tommei, G., Tortora, P., van Hoolst, T., Vokrouhlický, D., Watkins, M., Wu, X., Zannoni, M., 2021. Gravity, Geodesy and fundamental physics with BepiColombo's MORE investigation. Space Sci. Rev. 217 (1), 1–39. http://dx.doi.org/10.1007/s11214-021-00800-3.

Jacobstein, N., 2021. NASA's Perseverance: Robot laboratory on Mars. Science Robotics 6 (52), eabh3167. http://dx.doi.org/10.1126/scirobotics.abh3167.

Jakosky, B.M., 2021. Atmospheric loss to space and the history of water on Mars. Ann. Rev. Earth Planet. Sci. 49, http://dx.doi.org/10.1146/annurev-earth-062420-052845.

Karatekin, Ö., de Viron, O., Lambert, S., Dehant, V., Rosenblatt, P., Van Hoolst, T., Le Maistre, S., 2011. Atmospheric angular momentum variations of Earth, Mars and Venus at seasonal time scales. Planet. Space Sci. 59 (10), 923–933. http://dx.doi.org/10.1016/j.pss.2010.09.010.

Karatekin, Ö., Duron, J., Rosenblatt, P., Van Hoolst, T., Dehant, V., Barriot, J.P., 2005. Mars time-variable gravity and its determination: simulated geodesy experiments. J. Geophys. Res. (Planets) 110 (E6), E06001. http://dx.doi.org/10.1029/2004JE002378.

Karatekin, Ö., Van Hoolst, T., Dehant, V., 2006a. Martian global-scale CO_2 exchange from time-variable gravity measurements. J. Geophys. Res. (Planets) 111 (E6), E06003. http://dx.doi.org/10.1029/2005JE002591.

Karatekin, Ö., Van Hoolst, T., Tastet, J., de Viron, O., Dehant, V., 2006b. The effects of seasonal mass redistribution and interior structure on length-of-day variations of Mars. Adv. Space Res. 38 (4), 739–744. http://dx.doi.org/10.1016/j.asr.2005.03.117.

Kasevich, M., Chu, S., 1991. Atomic interferometry using stimulated Raman transitions. Phys. Rev. Lett. 67 (2), 181–184. http://dx.doi.org/10.1103/PhysRevLett.67.181.

Kayali, S., Morton, P., Gross, M., 2017. International challenges of GRACE follow-on. In: 2017 IEEE Aerospace Conference. 04.-11.03.2007, Big Sky, MT, USA, IEEE, pp. 1–8. http://dx.doi.org/10.1109/AERO.2017.7943615.

Klimczak, C., Kling, C.L., Byrne, P.K., 2018. Topographic expressions of large thrust faults on Mars. J. Geophys. Res. Planets 123 (8), 1973–1995. http://dx.doi.org/10.1029/2017JE005448.

Klinger, B., Mayer-Gürr, T., 2016. The role of accelerometer data calibration within GRACE gravity field recovery: Results from ITSG-Grace2016. Adv. Space Res. 58 (9), 1597–1609. http://dx.doi.org/10.1016/j.asr.2016.08.007.

Knapmeyer-Endrun, B., Panning, M., Bissig, F., Joshi, R., Khan, A., Kim, D., Lekić, V., Tauzin, B., Tharimena, S., Plasman, M., Compaire, N., Garcia, R., Margerin, L., Schimmel, M., Stutzmann, É., Schmerr, N., Bozdağ, E., Plesa, A., Wieczorek, M., Broquet, A., Antonangeli, D., McLennan, S., Samuel, H., Michaut, C., Pan, L., Smrekar, S., Johnson, C., Brinkman, N., Mittelholz, A., Rivoldini, A., Davis, P., Lognonné, P., Pinot, B., Scholz, J., Stähler, S., Knapmeyer, M., van Driel, M., Giardini, D., Banerdt, W., 2021. Thickness and structure of the Martian crust from InSight seismic data. Science 373, 438–443. http://dx.doi.org/10.1126/science.abf8966.

Koch, A., 2020. Link Acquisition and Optimization for Intersatellite Laser Interferometry (Ph.D. thesis). Leibniz Universität Hannover, http://dx.doi.org/10.15488/9799.

Koch, A., Sanjuan, J., Gohlke, M., Mahrdt, C., Brause, N., Braxmaier, C., Heinzel, G., 2018. Line of sight calibration for the laser ranging interferometer on-board the GRACE Follow-On mission: on-ground experimental validation. Opt. Express 26 (20), 25892–25908. http://dx.doi.org/10.1364/OE.26.025892.

Komatsu, G., Okubo, C.H., Wray, J.J., Ojha, L., Cardinale, M., Murana, A., Orosei, R., Chan, M.A., Ormö, J., Gallagher, C., 2016. Small edifice features in Chryse Planitia, Mars: Assessment of a mud volcano hypothesis. Icarus 268, 56–75. http://dx.doi.org/10.1016/j.icarus.2015.12.032.

Konopliv, A.S., Asmar, S.W., Folkner, W.M., Karatekin, Ö., Nunes, D.C., Smrekar, S.E., Yoder, C.F., Zuber, M.T., 2011. Mars high resolution gravity fields from MRO, Mars seasonal gravity, and other dynamical parameters. Icarus 211 (1), 401–428. http://dx.doi.org/10.1016/j.icarus.2010.10.004.

Konopliv, A.S., Park, R.S., Folkner, W.M., 2016. An improved JPL Mars gravity field and orientation from Mars orbiter and lander tracking data. Icarus 274, 253–260. http://dx.doi.org/10.1016/j.icarus.2016.02.052.

Konopliv, A.S., Park, R.S., Rivoldini, A., Baland, R.-M., Le Maistre, S., van Hoolst, T., Yseboodt, M., Dehant, V., 2020. Detection of the Chandler wobble of Mars from orbiting spacecraft. Geophys. Res. Lett. 47 (21), http://dx.doi.org/10.1029/2020GL090568.

Konopliv, A.S., Yoder, C.F., Standish, E.M., Yuan, D.-N., Sjogren, W.L., 2006. A global solution for the Mars static and seasonal gravity, Mars orientation, Phobos and Deimos masses, and Mars ephemeris. Icarus 182 (1), 23–50. http://dx.doi.org/10.1016/j.icarus.2005.12.025.

Kornfeld, R.P., Arnold, B.W., Gross, M.A., Dahya, N.T., Klipstein, W.M., Gath, P.F., Bettadpur, S., 2019. GRACE-FO: The gravity recovery and climate experiment follow-on mission. J. Spacecr. Rockets 56 (3), 931–951. http://dx.doi.org/10.2514/1.A34326.

Kuchynka, P., Folkner, W.M., Konopliv, A.S., Parker, T.J., Park, R.S., Le Maistre, S., Dehant, V., 2014. New constraints on Mars rotation determined from radiometric tracking of the opportunity Mars Exploration Rover. Icarus 229, 340–347. http://dx.doi.org/10.1016/j.icarus.2013.11.015.

Lachmann, M.D., Ahlers, H., Becker, D., Dinkelaker, A.N., Grosse, J., Hellmig, O., Müntinga, H., Schkolnik, V., Seidel, S.T., Wendrich, T., Wenzlawski, A., Carrick, B., Gaaloul, N., Lüdtke, D., Braxmaier, C., Ertmer, W., Krutzik, M., Lämmerzahl, C., Peters, A., Schleich, W.P., Sengstock, K., Wicht, A., Windpassinger, P., Rasel, E.M., 2021. Ultracold atom interferometry in space. Nature Commun. 12 (1), 1317. http://dx.doi.org/10.1038/s41467-021-21628-z.

Lainey, V., Pasewaldt, A., Robert, V., Rosenblatt, P., Jaumann, R., Oberst, J., Roatsch, T., Willner, K., Ziese, R., Thuillot, W., 2021. Mars moon ephemerides after 14 years of Mars Express data. Astron. Astrophys. 650, A64. http://dx.doi.org/10.1051/0004-6361/202039406.

Lan, S.Y., Kuan, P.C., Estey, B., Haslinger, P., Müller, H., 2012. Influence of the Coriolis force in atom interferometry. Phys. Rev. Lett. 108 (9), 090402. http://dx.doi.org/10.1103/PhysRevLett.108.090402.

Lauro, S.E., Pettinelli, E., Caprarelli, G., Guallini, L., Rossi, A.P., Mattei, E., Cosciotti, B., Cicchetti, A., Soldovieri, F., Cartacci, M., Di Paolo, F., Noschese, R., 2021. Multiple subglacial water bodies below the south pole of Mars unveiled by new MARSIS data. Nat. Astron. 5, 63–70. http://dx.doi.org/10.1038/s41550-020-1200-6, arXiv:2010.00870.

Lautier, J., Volodimer, L., Hardin, T., Merlet, S., Lours, M., Pereira Dos Santos, F., Landragin, A., 2014. Hybridizing matter-wave and classical accelerometers. Appl. Phys. Lett. 105 (14), 144102. http://dx.doi.org/10.1063/1.4897358.

Lemoine, F.G., Goossens, S., Sabaka, T.J., Nicholas, J.B., Mazarico, E., Rowlands, D.D., Loomis, B.D., Chinn, D.S., Caprette, D.S., Neumann, G.A., Smith, D.E., Zuber, M.T., 2013. High–degree gravity models from GRAIL primary mission data. J. Geophys. Res. Planets 118 (8), 1676–1698. http://dx.doi.org/10.1002/jgre.20118.

Lévèque, T., Fallet, C., Lefebve, J., Piquereau, A., Gauguet, A., Battelier, B., Bouyer, P., Gaaloul, N., Lachmann, M., Piest, B., Rasel, E., Müller, J., Schubert, C., Beaufils, Q., Santos, F.P.D., 2022. CARIOQA: Definition of a quantum pathfinder mission. In: Minoglou, K., Karafolas, N., Cugny, B. (Eds.), International Conference on Space Optics (ICSO) 2022. 3-7 October 2022, Dubrovnik, Croatia, In: Proceedings of SPIE, vol. 12777, SPIE, http://dx.doi.org/10.1117/12.2690536.

Lévèque, T., Fallet, C., Mandea, M., Biancale, R., Lemoine, J.M., Tavidel, S., Delavaul, S., Piquereau, A., Bourgogne, S., Pereira Dos Santos, F., Battelier, B., Bouyer, P., 2021. Gravity field mapping using laser-coupled quantum accelerometers in space. J. Geod. 95, 15. http://dx.doi.org/10.1007/s00190-020-01462-9.

Lognonné, P., Banerdt, W.B., Giardini, D., Pike, W., Christensen, U., Laudet, P., De Raucourt, S., Zweifel, P., Calcutt, S., Bierwirth, M., et al., 2019. SEIS: InSight's seismic experiment for internal structure of Mars. Space Sci. Rev. 215 (1), 12. http://dx.doi.org/10.1007/s11214-018-0574-6.

Louchet-Chauvet, A., Farah, T., Bodart, Q., Clairon, A., Landragin, A., Merlet, S., Pereira Dos Santos, F., 2011. The influence of transverse motion within an atomic gravimeter. New J. Phys. 13, 065025. http://dx.doi.org/10.1088/1367-2630/13/6/065025.

Lowry, A.R., Zhong, S., 2003. Surface versus internal loading of the Tharsis rise, Mars. J. Geophys. Res. Planets 108 (E9), 5099. http://dx.doi.org/10.1029/2003JE002111.

Mandea, M., Dehant, V., Cazenave, A., 2020. GRACE–gravity data for understanding the deep Earth's interior. Remote Sens. 12 (24), 4186. http://dx.doi.org/10.3390/rs12244186.

Mari, N., Hallis, L.J., Daly, L., Lee, M.R., 2020. Convective activity in a Martian magma chamber recorded by P-zoning in Tissint olivine. Meteorit. Planet. Sci. 55 (5), 1057–1072. http://dx.doi.org/10.1111/maps.13488.

McKenzie, D., Barnett, D.N., Yuan, D.-N., 2002. The relationship between Martian gravity and topography. Earth Planet. Sci. Lett. 195 (1), 1–16. http://dx.doi.org/10.1016/S0012-821X(01)00555-6.

Meister, J., Bremer, S., HosseiniArani, A., Leipner, A., List, M., Müller, J., Schilling, M., 2022. Reference mirror misalignment of cold atom interferometers on satellite-based gravimetry missions. In: 73rd International Astronautical Congress. IAC, 18-22 September 2022, Paris, France.

Ménoret, V., Vermeulen, P., Le Moigne, N., Bonvalot, S., Bouyer, P., Landragin, A., Desruelle, B., 2018. Gravity measurements below 10^{-9} g with a transportable absolute quantum gravimeter. Sci. Rep. 8 (1), 12300. http://dx.doi.org/10.1038/s41598-018-30608-1.

Métivier, L., Karatekin, Ö., Dehant, V., 2008. The effect of the internal structure of Mars on its seasonal loading deformations. Icarus 194 (2), 476–486. http://dx.doi.org/10.1016/j.icarus.2007.12.001.

Michalski, J.R., Cuadros, J., Niles, P.B., Parnell, J., Deanne Rogers, A., Wright, S.P., 2013. Groundwater activity on Mars and implications for a deep biosphere. Nature Geoscience 6 (2), 133–138. http://dx.doi.org/10.1038/ngeo1706.

Migliaccio, F., Batsukh, K., Benciolini, G.B., Braitenberg, C., Koç, Ö., Mottini, S., Pastorutti, A., Pivetta, T., Reguzzoni, M., Rosi, G., Rossi, L., Sorrentino, F., Tino, G.M., Vitti, A., 2022. Results of the MOCAST+ study on a quantum gravimetry mission. In: EGU General Assembly. 23.-27.05.2022, Vienna, Austria, http://dx.doi.org/10.5194/egusphere-egu22-9568.

Migliaccio, F., Reguzzoni, M., Batsukh, K., Tino, G.M., Rosi, G., Sorrentino, F., Braitenberg, C., Pivetta, T., Barbolla, D.F., Zoffoli, S., 2019. MOCASS: A satellite mission concept using cold atom interferometry for measuring the Earth gravity field. Surv. Geophys. 40 (5), 1029–1053. http://dx.doi.org/10.1007/s10712-019-09566-4.

Muirhead, B.K., Nicholas, A.K., Umland, J., Sutherland, O., Vijendran, S., 2020. Mars sample return campaign concept status. Acta Astronaut. 176, 131–138. http://dx.doi.org/10.1016/j.actaastro.2020.06.026.

Müller, V., Hauk, M., Misfeldt, M., Müller, L., Wegener, H., Yan, Y., Heinzel, G., 2022. Comparing GRACE-FO KBR and LRI ranging data with focus on carrier frequency variations. Remote Sens. 14 (17), 4335. http://dx.doi.org/10.3390/rs14174335.

Müntinga, H., Ahlers, H., Krutzik, M., Wenzlawski, A., Arnold, S., Becker, D., Bongs, K., Dittus, H., Duncker, H., Gaaloul, N., Gherasim, C., Giese, E., Grzeschik, C., Hänsch, T.W., Hellmig, O., Herr, W., Herrmann, S., Kajari, E., Kleinert, S., Lämmerzahl, C., Lewoczko-Adamczyk, W., Malcolm, J., Meyer, N., Nolte, R., Peters, A., Popp, M., Reichel, J., Roura, A., Rudolph, J., Schiemangk, M., Schneider, M.,

Seidel, S.T., Sengstock, K., Tamma, V., Valenzuela, T., Vogel, A., Walser, R., Wendrich, T., Windpassinger, P., Zeller, W., van Zoest, T., Ertmer, W., Schleich, W.P., Rasel, E.M., 2013. Interferometry with Bose-Einstein condensates in microgravity. Phys. Rev. Lett. 110, 093602. http://dx.doi.org/10.1103/PhysRevLett.110.093602.

Nazari-Sharabian, M., Aghababaei, M., Karakouzian, M., Karami, M., 2020. Water on Mars—a literature review. Galaxies 8 (2), 40. http://dx.doi.org/10.3390/galaxies8020040.

Nettleton, L.L., 1979. Quantitative analysis of a mud volcano gravity anomaly. Geophysics 44 (9), 1518. http://dx.doi.org/10.1190/1.1441022.

Neumann, G.A., Zuber, M.T., Wieczorek, M.A., McGovern, P.J., Lemoine, F.G., Smith, D.E., 2004. Crustal structure of Mars from gravity and topography. J. Geophys. Res. (Planets) 109 (E8), E08002. http://dx.doi.org/10.1029/2004JE002262, URL https://ui.adsabs.harvard.edu/abs/2004JGRE..109.8002N.

Oberst, J., Wickhusen, K., Gwinner, K., Hauber, E., Stark, A., Elgner, S., Grott, M., Fanara, L., Hussmann, H., Steinbrügge, G., Lewis, S., Balme, M., Maugeri, M., Diolaiuti, G., Karlsson, N., Johnsson, A., Ivanov, A., Hiesinger, H., 2022. Planetary polar explorer - the case for a next-generation remote sensing mission to low Mars orbit. Exp. Astron. http://dx.doi.org/10.1007/s10686-021-09820-x.

Oehler, D.Z., Allen, C.C., 2010. Evidence for pervasive mud volcanism in acidalia planitia, mars. Icarus 208 (2), 636–657. http://dx.doi.org/10.1016/j.icarus.2010.03.031.

Oehler, D.Z., Salvatore, M., Etiope, G., Allen, C.C., 2021. Focusing the search for organic biosignatures on Mars. In: 52nd Lunar and Planetary Science Conference. In: Lunar and Planetary Science Conference, p. 1353.

Orgel, C., Hauber, E., van Gasselt, S., Reiss, D., Johnsson, A., Ramsdale, J.D., Smith, I., Swirad, Z.M., Séjourné, A., Wilson, J.T., Balme, M.R., Conway, S.J., Costard, F., Eke, V.R., Gallagher, C., Kereszturi, Á., Łosiak, A., Massey, R.J., Platz, T., Skinner, J.A., Teodoro, L.F.A., 2019. Grid mapping the northern plains of Mars: A new overview of recent water- and ice-related landforms in Acidalia Planitia. J. Geophys. Res. (Planets) 124 (2), 454–482. http://dx.doi.org/10.1029/2018JE005664.

O'Rourke, J., Heinisch, P., Blum, J., Fornasier, S., Filacchione, G., Van Hoang, H., Ciarniello, M., Raponi, A., Gundlach, B., Blasco, R.A., et al., 2020. The Philae lander reveals low-strength primitive ice inside cometary boulders. Nature 586 (7831), 697–701. http://dx.doi.org/10.1038/s41586-020-2834-3.

Pail, R., Bingham, R., Braitenberg, C., Dobslaw, H., Eicker, A., Güntner, A., Horwath, M., Ivins, E., Longuevergne, L., Panet, I., Wouters, B., IUGG Expert Panel, 2015. Science and user needs for observing global mass transport to understand global change and to benefit society. Surv Geophy 36 (6), 743–772. http://dx.doi.org/10.1007/s10712-015-9348-9.

Peddinti, D.A., McNamara, A.K., 2019. Dynamical investigation of a thickening ice-shell: Implications for the icy moon Europa. Icarus 329, 251–269. http://dx.doi.org/10.1016/j.icarus.2019.03.037.

Peters, A., Chung, K.Y., Chu, S., 1999. Measurement of gravitational acceleration by dropping atoms. Nature 400, 849–852. http://dx.doi.org/10.1038/23655.

Petricca, F., Genova, A., Goossens, S., Iess, L., Spada, G., 2022. Constraining the internal structures of Venus and Mars from the gravity response to atmospheric loading. Planet. Sci. J. 3 (7), 164. http://dx.doi.org/10.3847/PSJ/ac7878.

Phillips, R.J., Zuber, M.T., Solomon, S.C., Golombek, M.P., Jakosky, B.M., Banerdt, W.B., Smith, D.E., Williams, R.M.E., Hynek, B.M., Aharonson, O., Hauck, II, S.A., 2001. Ancient geodynamics and global-scale hydrology on Mars. Science 291 (5513), 2587–2591. http://dx.doi.org/10.1126/science.1058701.

Pou, L., Nimmo, F., Rivoldini, A., Khan, A., Bagheri, A., Gray, T., Samuel, H., Lognonné, P., Plesa, A.-C., Gudkova, T., et al., 2022. Tidal constraints on the Martian interior. J. Geophys. Res. Planets 127 (11), e2022JE007291. http://dx.doi.org/10.1029/2022JE007291.

Rakholia, A.V., McGuinness, H.J., Biedermann, G.W., 2014. Dual-axis high-data-rate atom interferometer via cold ensemble exchange. Phys. Rev. Appl. 2 (5), 054012. http://dx.doi.org/10.1103/PhysRevApplied.2.054012.

Rees, E.R., Wade, A.R., Sutton, A.J., McKenzie, K., 2022. Absolute frequency readout of cavity against atomic reference. Remote Sens. 14 (11), 2689. http://dx.doi.org/10.3390/rs14112689.

Rees, E.R., Wade, A.R., Sutton, A.J., Spero, R.E., Shaddock, D.A., McKenzie, K., 2021. Absolute frequency readout derived from ULE cavity for next generation geodesy missions. Opt. Express 29 (16), 26014–26027. http://dx.doi.org/10.1364/OE.434483.

Richardson, L.L., Rajagopalan, A., Albers, H., Meiners, C., Nath, D., Schubert, C., Tell, D., Wodey, É., Abend, S., Gersemann, M., Ertmer, W., Rasel, E.M., Schlippert, D., Mehmet, M., Kumanchik, L., Colmenero, L., Spannagel, R., Braxmaier, C., Guzmán, F., 2020. Optomechanical resonator-enhanced atom interferometry. Commun. Phys. 3 (1), 208. http://dx.doi.org/10.1038/s42005-020-00473-4.

Rivoldini, A., Van Hoolst, T., Verhoeven, O., Mocquet, A., Dehant, V., 2011. Geodesy constraints on the interior structure and composition of Mars. Icarus 213 (2), 451–472. http://dx.doi.org/10.1016/j.icarus.2011.03.024.

Root, B., Fullea, J., Ebbing, J., Martinec, Z., 2021. Combining the deep earth and lithospheric gravity field to study the density structure of the upper mantle. In: EGU General Assembly. 19.-30.04.2021, Vienna, Austria, http://dx.doi.org/10.5194/egusphere-egu21-2950.

Root, B., Novák, P., Dirkx, D., Kaban, M., van der Wal, W., Vermeersen, L., 2016. On a spectral method for forward gravity field modelling. J. Geodyn. 97, 22–30. http://dx.doi.org/10.1016/j.jog.2016.02.008.

Root, B., Qin, W., 2022. A re-analysis of the lithospheric flexure on Mars. In: Europlanet Science Congress, Vol. 16. 2022, 18.-23.09.2022, Granada, Spain, http://dx.doi.org/10.5194/epsc2022-375.

Root, B.C., Sebera, J., Szwillus, W., Thieulot, C., Martinec, Z., Fullea, J., 2022. Benchmark forward gravity schemes: the gravity field of a realistic lithosphere model WINTERC-G. Solid Earth 13 (5), 849–873. http://dx.doi.org/10.5194/se-13-849-2022.

Root, B.C., van der Wal, W., Novák, P., Ebbing, J., Vermeersen, L.L.A., 2015. Glacial isostatic adjustment in the static gravity field of Fennoscandia. J. Geophys. Res. Solid Earth 120 (1), 503–518. http://dx.doi.org/10.1002/2014JB011508.

Rosen, M.D., 2021. Analysis of Hybrid Satellite-To-Satellite Tracking and Quantum Gravity Gradiometry Architecture for Time-Variable Gravity Sensing Missions (Ph.D. thesis). The University of Texas at Austin, http://dx.doi.org/10.26153/tsw/14541.

Rudolph, J., Herr, W., Grzeschik, C., Sternke, T., Grote, A., Popp, M., Becker, D., Müntinga, H., Ahlers, H., Peters, A., 2015. A high-flux BEC source for mobile atom interferometers. New J. Phys. 17, 065001. http://dx.doi.org/10.1088/1367-2630/17/6/065001.

Rummel, R., Yi, W., Stummer, C., 2011. GOCE gravitational gradiometry. J. Geod. 85, 777–790. http://dx.doi.org/10.1007/s00190-011-0500-0.

Sanjuan, J., Abich, K., Gohlke, M., Resch, A., Schuldt, T., Wegehaupt, T., Barwood, G.P., Gill, P., Braxmaier, C., 2019. Long-term stable optical cavity for special relativity tests in space. Optics Express 27 (25), 36206–36220. http://dx.doi.org/10.1364/OE.27.036206.

Savoie, D., Altorio, M., Fang, B., Sidorenkov, L.A., Geiger, R., Landragin, A., 2018. Interleaved atom interferometry for high-sensitivity inertial measurements. Sci. Adv. 4, http://dx.doi.org/10.1126/sciadv.aau7948.

Schütze, D., Stede, G., Müller, V., Gerberding, O., Bandikova, T., Sheard, B.S., Heinzel, G., Danzmann, K., 2014. Laser beam steering for GRACE Follow-On intersatellite interferometry. Opt. Express 22 (20), 24117–24132. http://dx.doi.org/10.1364/OE.22.024117.

Seu, R., Phillips, R.J., Biccari, D., Orosei, R., Masdea, A., Picardi, G., Safaeinili, A., Campbell, B.A., Plaut, J.J., Marinangeli, L., Smrekar, S.E., Nunes, D.C., 2007. SHARAD sounding radar on the Mars Reconnaissance Orbiter. J. Geophys. Res. Planets 112, E05S05. http://dx.doi.org/10.1029/2006JE002745.

Skinner, J.A., Tanaka, K.L., 2007. Evidence for and implications of sedimentary diapirism and mud volcanism in the southern Utopia highland lowland boundary plain, Mars. Icarus 186 (1), 41–59. http://dx.doi.org/10.1016/j.icarus.2006.08.013.

Smirnov, V.M., Yushkova, O.V., Karachevtseva, I.P., Nadezhdina, I.E., 2014. The influence of relief on formation of reflected signals of subsurface sounding radar. Solar System Research 48 (3), 176–181. http://dx.doi.org/10.1134/S003809461403006X.

Smith, M.D., 2009. THEMIS observations of Mars aerosol optical depth from 2002–2008. Icarus 202 (2), 444–452. http://dx.doi.org/10.1016/j.icarus.2009.03.027.

Smith, I.B., Lalich, D.E., Rezza, C., Horgan, B.H.N., Whitten, J.L., Nerozzi, S., Holt, J.W., 2021. A solid interpretation of bright radar reflectors under the Mars south polar ice. Geophys. Res. Lett. 48 (15), e93618. http://dx.doi.org/10.1029/2021GL093618.

Smith, D.E., Zuber, M.T., Neumann, G.A., 2001. Seasonal variations of snow depth on Mars. Science 294 (5549), 2141–2146. http://dx.doi.org/10.1126/science.1066556.

Stähler, S.C., Khan, A., Banerdt, W.B., Lognonné, P., Giardini, D., Ceylan, S., Drilleau, M., Duran, A.C., Garcia, R.F., Huang, Q., Kim, D., Lekic, V., Samuel, H., Schimmel, M., Schmerr, N., Sollberger, D., Stutzmann, É., Xu, Z., Antonangeli, D., Charalambous, C., Davis, P.M., Irving, J.C.E., Kawamura, T., Knapmeyer, M., Maguire, R., Marusiak, A.G., Panning, M.P., Perrin, C., Plesa, A.-C., Rivoldini, A., Schmelzbach, C., Zenhäusern, G., Beucler, É., Clinton, J., Dahmen, N., van Driel, M., Gudkova, T., Horleston, A., Pike, W.T., Plasman, M., Smrekar, S.E., 2021. Seismic detection of the Martian core. Science 373 (6553), 443–448. http://dx.doi.org/10.1126/science.abi7730.

Stamenkovic, V., Lynch, K., Boston, P., Tarnas, J., Edwards, C.D., Sherwood-Lollar, B., Atreya, S., Templeton, A., Freeman, A., Fischer, W., Spohn, T., Webster, C., Fairén, A.G., Mustard, J.J., Mischna, M., Onstott, T.C., Osburn, M.R., Kieft, T., Grimm, R.E., Brinckerhoff, W.B., Johnson, S., Beegle, L., Head, J., Haldemann, A., Cockell, C., Hernlund, J., Wilcox, B., Paige, D., Etiope, G., Glavin, D., Zorzano, M.-P., Sekine, Y., Fabien, S., Kirschvink, J., Magnabosco, C., Orosei, R., Grott, M., Rummel, J.D., Kobayashi, A., Inagaki, F., Bishop, J., Chevrier, V., Bell, M.S., Orcutt, B.N., McIntosh, J., Miljkovic, K., Breuer, D., Usui, T., Zacny, K., Heggy, E., Rivera-Valentín, E.G., Barba, N.J., Woolley, R., Warr, O., Malaska, M., Blank, J.G., Ruffatto, D.F., Sapers, H.M., Matthies, L.H., Ward, L., Shkolyar, S., Schmelzbach, C., Gabriel, T.S.J., Parker, C., Bolivar-Torres, H.H., Pál, B., Schulze-Makuch, D., Torres Celis, J.A., Keresztúri, A., Spry, J.A., Uckert, K., Hesse, M.A., Harris, R., Plesa, A.-C., Hu, R., Agha-mohammadi, A.-a., Wade, B.D., Chatterjee, S., McGarey, P., Graham, H.V., Suzuki, S., Schrenk, M., Sherrill, K., Howe, S., Manthena, R., Burgin, M., Carpenter, P., Giersch, L., Cormarkovic, V., Smith, N., McDonnell, J.J., Michalski, J., Jha, D., Cable, M.L., Gloesener, E., Paul, V., Gault, S., Kedar, S., Marteau, E., Temel, O., Krieger, S., Timoney, R., 2021. Deep trek: Science of subsurface habitability & life on Mars. In: Bulletin of the American Astronomical Society, Vol. 53. p. 250. http://dx.doi.org/10.3847/25c2cfeb.dc18f731.

Starichenko, E.D., Belyaev, D.A., Medvedev, A.S., Fedorova, A.A., Korablev, O.I., Trokhimovskiy, A., Yiğit, E., Alday, J., Montmessin, F., Hartogh, P., 2021. Gravity wave activity in the Martian atmosphere at altitudes 20–160 km from ACS/TGO occultation measurements. J. Geophys. Res. Planets 126 (8), e2021JE006899. http://dx.doi.org/10.1029/2021JE006899.

Steffen, H., Gitlein, O., Denker, H., Müller, J., Timmen, L., 2009. Present rate of uplift in Fennoscandia from GRACE and absolute gravimetry. Tectonophysics 474 (1-2), 69–77. http://dx.doi.org/10.1016/j.tecto.2009.01.012.

Sutton, A., Mckenzie, K., Ware, B., Shaddock, D.A., 2010. Laser ranging and communications for LISA. Optics Express 18 (20), 20759–20773. http://dx.doi.org/10.1364/OE.18.020759.

Tapley, B.D., Bettadpur, S., Ries, J.C., Thompson, P.F., Watkins, M.M., 2004. GRACE measurements of mass variability in the Earth system. Science 305 (5683), 503–505. http://dx.doi.org/10.1126/science.1099192.

Tapley, B.D., Watkins, M.M., Flechtner, F., Reigber, C., Bettadpur, S., Rodell, M., Sasgen, I., Famiglietti, J.S., Landerer, F.W., Chambers, D.P., Reager, J.T., Gardner, A.S., Save, H., Ivins, E.R., Swenson, S.C., Boening, C., Dahle, C., Wiese, D.N., Dobslaw, H., Tamisiea, M.E., Velicogna, I., 2019. Contributions of GRACE to understanding climate change. Nature Clim. Change 9 (5), 358–369. http://dx.doi.org/10.1038/s41558-019-0456-2.

Thompson, R., Folkner, W.M., deVine, G., Klipstein, W.M., McKenzie, K., Spero, R., Yu, N., Stephens, M., Leitch, K., Pierce, R., Lam, T.T.-Y., Shaddock, D.A., 2011. A flight-like optical reference cavity for GRACE follow-on laser frequency stabilization. In: 2011 Joint Conference of the IEEE International Frequency Control and the European Frequency and Time Forum (FCS) Proceedings, Vol. 10562. 02.-05.05.2011, San Francisco, Tx, USA, http://dx.doi.org/10.1109/FCS.2011.5977873.

Touboul, P., Foulon, B., Christophe, B., Marque, J.P., 2012. CHAMP, GRACE, GOCE instruments and beyond. In: Kenyon, S., Pacino, M.C., Marti, U. (Eds.), Geodesy for Planet Earth. In: IAG Symposia, vol. 136, Springer, Berlin, Heidelberg, pp. 215–221. http://dx.doi.org/10.1007/978-3-642-20338-1_26.

Trimeche, A., Battelier, B., Becker, D., Bertoldi, A., Bouyer, P., Braxmaier, C., Charron, E., Corgier, R., Cornelius, M., Douch, K., Gaaloul, N., Herrmann, S., Müller, J., Rasel, E., Schubert, C., Wu, H., Pereira dos Santos, F., 2019. Concept study and preliminary design of a cold atom interferometer for space gravity gradiometry. Classical Quantum Gravity 36 (21), 215004. http://dx.doi.org/10.1088/1361-6382/ab4548.

Turcotte, D.L., Willemann, R.J., Haxby, W.F., Norberry, J., 1981. Role of membrane stresses in the support of planetary topography. J. Geophys. Res. Solid Earth 86 (B5), 3951–3959. http://dx.doi.org/10.1029/JB086iB05p03951.

van Brummen, B., 2022. Mars Gravity Inversion: Investigating the lateral density variations of the Martian lithosphere (Master's thesis). Delft University of Technology, URL http://resolver.tudelft.nl/uuid:1f8beaf8-a97a-47d5-a57b-38b91a35bec9.

van Zoest, T., Gaaloul, N., Singh, Y., Ahlers, H., Herr, W., Seidel, S.T., Ertmer, W., Rasel, E., Eckart, M., Kajari, E., Arnold, S., Nandi, G., Schleich, W.P., Walser, R., Vogel, A., Sengstock, K., Bongs, K., Lewoczko-Adamczyk, W., Schiemangk, M., Schuldt, T., Peters, A., Könemann, T., Müntinga, H., Lämmerzahl, C., Dittus, H., Steinmetz, T., Hänsch, T.W., Reichel, J., 2010. Bose-Einstein condensation in microgravity. Science 328, 1540–1543. http://dx.doi.org/10.1126/science.1189164.

Warner, M., Grosse, J., Wörner, L., Kumanchik, L., Knoop, D., Schröder, J., Halbey, J., Riesner, R., Braxmaier, C., 2019. Hybrid inertial sensors – future prospects of inertial sensors based on atom interferometry fused with opto-mechanical accelerometers. In: 2019 DGON Inertial Sensors and Systems. ISS, pp. 1–14. http://dx.doi.org/10.1109/ISS46986.2019.8943706.

Watts, A., Burov, E., 2003. Lithospheric strength and its relationship to the elastic and seismogenic layer thickness. Earth Planet. Sci. Lett. 213 (1), 113–131. http://dx.doi.org/10.1016/S0012-821X(03)00289-9.

Wieczorek, M.A., Broquet, A., McLennan, S.M., Rivoldini, A., Golombek, M., Antonangeli, D., Beghein, C., Giardini, D., Gudkova, T., Gyalay, S., Johnson, C.L., Joshi, R., Kim, D., King, S.D., Knapmeyer-Endrun, B., Lognonné, P., Michaut, C., Mittelholz, A., Nimmo, F., Ojha, L., Panning, M.P., Plesa, A.-C., Siegler, M.A., Smrekar, S.E., Spohn, T., Banerdt, W.B., 2022. InSight constraints on the global character of the Martian crust. J. Geophys. Res. (Planets) 127 (5), e07298. http://dx.doi.org/10.1029/2022JE007298.

Williams, J.G., Konopliv, A.S., Boggs, D.H., Park, R.S., Yuan, D.-N., Lemoine, F.G., Goossens, S., Mazarico, E., Nimmo, F., Weber, R.C., et al., 2014. Lunar interior properties from the GRAIL mission. J. Geophys. Res. Planets 119 (7), 1546–1578. http://dx.doi.org/10.1002/2013JE004559.

Xiao, H., Stark, A., Schmidt, F., Hao, J., Steinbrügge, G., Wagner, N.L., Su, S., Cheng, Y., Oberst, J., 2022a. Spatio–Temporal level variations of the Martian seasonal north polar cap from co–registration of MOLA profiles. J. Geophys. Res. Planets 127 (10), http://dx.doi.org/10.1029/2021JE007158.

Xiao, H., Stark, A., Schmidt, F., Hao, J., Su, S., Steinbrügge, G., Oberst, J., 2022b. Spatio–Temporal level variations of the Martian seasonal south polar cap from co–registration of MOLA profiles. J. Geophys. Res. Planets 127 (7), http://dx.doi.org/10.1029/2022JE007196.

Yoder, C.F., Konopliv, A.S., Yuan, D.N., Standish, E.M., Folkner, W.M., 2003. Fluid core size of Mars from detection of the solar tide. Science 300 (5617), 299–303. http://dx.doi.org/10.1126/science.1079645.

Zahzam, N., Christophe, B., Lebat, V., Hardy, E., Huynh, P.-A., Marquet, N., Blanchard, C., Bidel, Y., Bresson, A., Abrykosov, P., Gruber, T., Pail, R., Daras, I., Carraz, O., 2022. Hybrid electrostatic-atomic accelerometer for future space gravity missions. Remote Sens. 14 (14), http://dx.doi.org/10.3390/rs14143273.

Zhong, S., Roberts, J.H., 2003. On the support of the Tharsis Rise on Mars. Earth Planet. Sci. Lett. 214 (1), 1–9. http://dx.doi.org/10.1016/S0012-821X(03)00384-4.

Zhong, S., Zhang, N., Li, Z.-X., Roberts, J.H., 2007. Supercontinent cycles, true polar wander, and very long-wavelength mantle convection. Earth Planet. Sci. Lett. 261 (3), 551–564. http://dx.doi.org/10.1016/j.epsl.2007.07.049.

Zingerle, P., Pail, R., Gruber, T., Oikonomidou, X., 2020. The combined global gravity field model XGM2019e. J. Geod. 94 (7), 66. http://dx.doi.org/10.1007/s00190-020-01398-0.

Zuber, M.T., Smith, D.E., Watkins, M.M., Asmar, S.W., Konopliv, A.S., Lemoine, F.G., Melosh, H.J., Neumann, G.A., Phillips, R.J., Solomon, S.C., et al., 2013. Gravity field of the Moon from the Gravity Recovery and Interior Laboratory (GRAIL) mission. Science 339 (6120), 668–671. http://dx.doi.org/10.1126/science.1231507.

Zuber, M.T., Solomon, S.C., Phillips, R.J., Smith, D.E., Tyler, G.L., Aharonson, O., Balmino, G., Banerdt, W.B., Head, J.W., Johnson, C.L., Lemoine, F.G., McGovern, P.J., Neumann, G.A., Rowlands, D.D., Zhong, S., 2000. Internal structure and early thermal evolution of Mars from Mars Global Surveyor topography and gravity. Science 287 (5459), 1788–1793. http://dx.doi.org/10.1126/science.287.5459.1788.

Zurek, R.W., Tolson, R.A., Bougher, S.W., Lugo, R.A., Baird, D.T., Bell, J.M., Jakosky, B.M., 2017. Mars thermosphere as seen in MAVEN accelerometer data. J. Geophys. Res. (Space Phys.) 122 (3), 3798–3814. http://dx.doi.org/10.1002/2016JA023641.